On-Line Appendices to

Thermal Radiation Heat Transfer

John R. Howell, M. Pinar Menguc, and Robert Siegel
6th Edition, Taylor and Francis, 2015

Appendix A. Wide-Band Models

A.1 Wide-Band Models and Correlations

Edwards and Menard (1964) modeled a band of rotation lines that are reordered in wave number so they form an array with exponentially decreasing line intensities moving away from the band center, and covering the entire band. This is the *exponential wide-band* model. Edwards and co-workers [Edwards (1960,1962,1965), Edwards and Menard (1964a,b), Edwards and Sun (1964), Edwards et al. (1965), Edwards and Nelson (1962), Edwards and Balakrishnan (1973), Weiner (1966), Hines and Edwards (1968)] assembled a large body of data on the important radiating gases at typical engineering conditions. By comparing their band-correlation relations with data over large ranges of pressure and temperature, they determined empirically how the physical variables are related to the effective bandwidth $\bar{A}_l(T)$, to an effective bandwidth parameter $\omega(T)$, and to a modified pressure-broadening parameter $B(T, P_e)$, where P_e is the effective broadening pressure. The μ was expressed in the form of a modified variable $u = X\alpha/\omega$, that is in terms of the mass path length $X = \rho S$ of the absorbing gas component and a quantity $\alpha(T)$ that will be determined. Available correlations are summarized in Table A.1.

TABLE A.1
Available Band Absorptance Correlations for Isothermal Media

Gas	Bands	Reference	Comments	Type of Correlation
CO_2	2.0, 2.7, 4.3, 9.4, 10.4, and 15 μm	Table 9.3 [Marin and Buckius (1998b)]	Wide-band $300 < T < 1390$ K $0.1 < X < 23{,}000$ g/m^2	*c-k* wide-band distribution
	WSGG (all)	Table 9.7 [Denison and Webb (1995)]	$400 < T < 2500$ K 3×10^{-5} to 600 m^2/mol	Spectral line WSGG
	2.0, 2.7, 4.3, 9.4, 10.4, and 15 μm	[Domoto (1974)]	$300 < T < 1390$ K $0.1 < X < 23{,}000$ g/m^2	*k*-distribution (wide-band)
	2.7,4.3, and 15 μm	[Chu and Greif (1978)]	$T \approx 300$ K $0.1 < X < 23{,}000$ g/m^2	Nonrigid rotator spectroscopic wide band
	2.7 μm	[Lin and Greif (1974)]	$T \approx 300$ K $0.081 < pS < 1300$ atm ⇖cm	Rigid rotator spectroscopic wide band
	2.0, 2.7, 4.3, and 15 μm	Table 9.2 [Edwards (1976); Edwards and Menard (1964b); Edwards and Balakrishnan (1973); Edwards et al. (1967)]	$300 < T < 1390$ K $0.1 < X < 23{,}000$ g/m^2	Exponential wide band
	9.4 and 10.4 μm	Table 9.2 [Edwards (1976); Edwards and Menard (1964); Edwards and Balakrishnan (1973); Edwards et al. (1967)]	$300 < T < 1390$ K $0.1 < X < 23{,}000$ g/m^2	Exponential wide band
	2.0, 2.7, 4.3, 9.4, 10.4, and 15 μm	[Edwards (1960)]	$300 < T < 1390$ K $0.1 < X < 23{,}000$ g/m^2	Equivalent bandwidth
H_2O	1.38, 1.87, 2.7, and 6.3 μm, rotational	Table 9.4 [Marin and Buckius (1998a)]	$300 < T < 2900$ K (except rotational band, $300 < T < 1900$ K) $10^{-5} < pS < 10^4$ atm ⇖m	*c-k* (wide-band) distribution
	WSGG (all)	Table 9.5 [Denison and Webb (1993)]	$400 < T < 2500$ K 3×10^{-5} to 60 m^2/mol	Spectral line WSGG
	1.38, 1.87, 2.7, and 6.3 μm, rotational	[Kamiuto and Tokita (1994)]	$300 < T < 3000$ K $0.1 < pS < 1000$ bar ⇖cm	Modified exponential wide band
	2.7 μm	[Lin and Greif (1974)]	$T = 300$ K $3.3 < pS < 2800$ atm ⇖cm	Rigid rotator spectroscopic wide band
	2.7 and 6.3 μm	[Weiner (1966)]	$300 < T < 1100$ K $1 < X < 21000$ g/m^2	Equivalent line
	1.38, 1.87, 2.7, and 6.3 μm	Table 9.2 [Edwards (1976); Edwards et al. (1965); Edwards and Balakrishnan (1973); Edwards et al. (1967)]]	$300 < T < 2250$ K $1 < X < 38{,}000$ g/m^2	Exponential wide band
	Rotational band ($\kappa > 10$ μm)	[Charalampopoulos and Felske (1983)]	$500 < T < 2400$ K $1.5 < pS < 30$ atm ⇖cm	Exponential wide band

[a] Varies with band.

TABLE A.1 (CONTINUED)
Available Band Absorptance Correlations for Isothermal Media

Gas	Bands	Reference	Comments	Type of Correlation
CO	WSGG (all bands)	Solovjov and Webb (1998)]	$300 < T < 2500$ K	Spectral line WSGG
	2.35 and 4.67 μm	Table 9.2 [Edwards (1976); Edwards and Menard (1964b); Edwards and Balakrishnan (1973)]	$300 < T < 1500$ K (2.35) $300 < T < 1800$ K (4.67) $19 < X < 650$ g/m^2	Exponential wide band
	4.7 μm	[Hsieh and Greif (1972); Hashemi et al. (1976); Chu and Greif (1978)]	$300 < T < 1800$ K $19 < X < 650$ g/m^2	Rigid and nonrigid rotator spectroscopic wide-band model
CH_4	1.71, 2.37, 3.31, and 7.66 μm	Table 9.2 [Edwards (1976); Edwards and Menard (1964b); Edwards and Balakrishnan (1973)]	$300 < T < 1000$ K[a] $19 < X < 650$ g/m^2	Exponential wide band
HCl		[Stull and Plass (1960a)]	1000–3400 cm^{-1}	Spectral emittance
SO_2	4.00, 4.34, 5.33, 7.35, 8.68, and 19.27 μm	[Kunitomo et al. (1981)]	$300 < T < 2000$ K $0.06 < pS < 180$ atm-cm	Statistical narrow band and exponential wide band
	4.00, 4.34, 7.35, 8.68, and 19.27 μm	[Chan and Tien (1971)]	$500 < T < 3500$°R $0.002 < pS < 2$ atm-ft	Elsasser narrow band and exponential wide band
H_2		[Aroeste and Benton (1956)]	Not correlated-presented in terms of spectral and total emittance	
Atmospheric gases—N_2, O_2, CO_2, O_3, H_2O, CH_3, and nitrogen oxides		[Goody and Yung (1989)]	Discussion of literature up to 1960	
Air	All important contributing bands	[Bond et al (1965)]	The citation [Bond et al. (1965)] provides references up to 1965 for data to calculate band absorptance	
NH_3	3.0, 10.5, 2.9, and 6.15 μm	[Tien (1973)]	$T < 300$ K $2 < X < 312$ g/m^2	Exponential wide band
NO	5.35 μm	[Hashemi et al. (1976); Chu and Greif (1978)]	$T < 300$ K $0.845 < pS < 12.56$ atm-cm	Rigid and nonrigid rotator spectroscopic wide-band model
N_2O	4.5 μm	[Chu and Greif (1978)]	$T < 303$ K $0.0186 < pS < 76.4$ atm-cm	Nonrigid rotator spectroscopic wide-band model
CCl_4 (liquid)	All important	[Novotny et al. (1974)]		Two-parameter Elsasser and statistical narrow band

[a] Varies with band.

TABLE A.1 (CONTINUED)
Available Band Absorptance Correlations for Isothermal Media

Gas	Bands	Reference	Comments	Type of Correlation
H_2, N_2, O_2, CH_4, CO, Ar (liquids only)	All important far-infrared bands in 40 to 500 μm region; for H_2, 16.7 to 500 μm	[Jones (1970)]	T near normal boiling point at 1 atm, S = 1.27 and 2.54 cm, plus 3.25 cm for H_2	Data for absorption coefficient versus wave number
C_2H_2	Wave number, (cm^{-1}) 3287; 1328, 729	[Brosmer and Tien (1985)]	Discussion of literature; measurements from T = 290 to 600 K	Exponential wide band
C_2H_4	Four in infrared	[Tuntomo et al. (1989)]	Measurements and correlation	Statistical narrow band, wide band

[a] Varies with band.

A brief description of the exponential wide band correlation is given here for the four gases in Table A.2. Information for NO and SO_2 is in Edwards and Balakrishnan (1973) [see also Edwards (1976)]. The correlation is in terms of three quantities: α, the integrated band intensity; B, the line-width parameter; and ω, the bandwidth parameter. The desired total band absorption $\bar{A}$ is found from the following correlations (the band subscript l on $\bar{A}$ has been dropped for convenience):

$$\text{For } B<1: \quad \left.\begin{aligned} \bar{A} &= \omega u && 0 \le u \le B \\ \bar{A} &= \omega(2\sqrt{Bu} - B) && B \le u \le \frac{1}{B} \\ \bar{A} &= \omega[\ln(Bu) + 2 - B] && \frac{1}{B} \le u \le \infty \end{aligned}\right\} \tag{A.1a}$$

$$\text{For } B \ge 1: \quad \left.\begin{aligned} \bar{A} &= \omega u && 0 \le u \le 1 \\ \bar{A} &= \omega(\ln u + 1) && 1 \le u \le \infty \end{aligned}\right\} \tag{A.1b}$$

The B is π times the ratio of mean line width to spacing, i.e., the parameter β adjusted for broadening effects, including pressure broadening: $B = \beta P_e$, where $P_e = [P/P_0 + (p/P_0)(b-1)]^n$, P is the total pressure (atm) of radiating and nonradiating gas, P_0 =1 atm, and p is the partial pressure of the radiating gas ($p_e \to 1$ as $p_e \to 0$ and $P \to P_0$). The b and n are in Table A.2 for each gas band. The $u = X\alpha/\omega$, where X is the mass path length of the radiating gas. The ω is found from $\omega = \omega_0 (T/T_0)^{1/2}$, where ω_0 is in Table A.2 and T_0 = 100 K. The table also gives the quantities necessary to obtain α and β from the following:

$$\alpha(T) = \alpha_0 \frac{1 - \exp\left(-\sum_{k=1}^{m} u_k \delta_k\right)}{1 - \exp\left(-\sum_{k=1}^{m} u_{0,k} \delta_k\right)} \left[\frac{\Psi(T)}{\Psi(T_0)}\right] \tag{A.2a}$$

$$\beta(T) = \beta_0 \left(\frac{T_0}{T} \right)^{1/2} \frac{\Phi(T)}{\Phi(T_0)} \tag{A.2b}$$

where

$$\Psi(T) = \frac{\prod_{k=1}^{m} \sum_{\upsilon_k=\upsilon_{0,k}}^{\infty} \left\{ \left(\upsilon_k + g_k + |\delta_k| - 1 \right)! / \left[\left(g_k - 1 \right)! \upsilon_k ! \right] \right\} e^{-u_k \upsilon_k}}{\prod_{k=1}^{m} \sum_{\upsilon_k=0}^{\infty} \left\{ \left(\upsilon_k + g_k - 1 \right)! / \left[\left(g_k - 1 \right)! \upsilon_k ! \right] \right\} e^{-u_k \upsilon_k}} \tag{A.2c}$$

$$\Phi(T) = \frac{\left[\prod_{k=1}^{m} \sum_{\upsilon_k=\upsilon_{0,k}}^{\infty} \left(\left\{ \left(\upsilon_k + g_k + |\delta_k| - 1 \right)! / \left[\left(g_k - 1 \right)! \upsilon_k ! \right] \right\} e^{-u_k \upsilon_k} \right)^{1/2} \right]^2}{\prod_{k=1}^{m} \sum_{\upsilon_k=\upsilon_{0,k}}^{\infty} \left\{ \left(\upsilon_k + g_k + |\delta_k| - 1 \right)! / \left[\left(g_k - 1 \right)! \upsilon_k ! \right] \right\} e^{-u_k \upsilon_k}} \tag{A.2d}$$

in which

$$u_k = \frac{hc\eta_k}{kT}, \qquad u_{0,k} = \frac{hc\eta_k}{kT_0}$$

and $\upsilon_{0,k} = 0$ if δ_k is positive or zero and is $|\delta_k|$ if δ_k is negative. Some illustrative numerical examples are in Edwards (1976) and Example A.1.

TABLE A.2
Exponential Wide-Band Parameters

				Pressure Parameters (T_o = 100 K)				
Gas $m, \eta\,(cm^{-1}), g$	Band (μm)	Band Center η (cm^{-1})	$\delta_1 \ldots . \delta_m$	b	n	α_o (cm^{-1}/g m^{-2})	β_o	ω_0 (cm^{-1})
CO_2	15	667	0, 1, 0	1.3	0.7	19.0	0.06157	12.7
m = 3, η = 1351, g_1 = l	10.4	960	−1, 0, 1	1.3	0.8	2.47 x 10^{-9}	0.04017	13.4
η = 667, g_1 = 2	9.4	1060	0, −2, 1[b]	1.3	0.8	2.48 x 10^{-9}[b]	0.11888[b]	10.1
η = 2396, g_3 = l	4.3	2410[a]	0, 0, 1	1.3	0.8	110.0	0.24723	11.2
	2.7	3660	1, 0, 1	1.3	0.65	4.0	0.13341	23.5
	2.0	5200	2, 0, 1	1.3	0.65	0.066	0.39305	34.5
CH_4	7.66	1310	0, 0, 0, 1	1.3	0.8	28.0	0.08698	21.0
m = 4, η_1 = 2914, g_1 = 1	3.31	3020	0, 0, 1, 0	1.3	0.8	46.0	0.06973	56.0
η_2 =1526, g_2 = 2	2.37	4220	1, 0, 0, 1	1.3	0.8	2.9	0.35429	60.0

η_3 =3020, g_3 = 3	1.71	5861	1, 1, 0, 1	1.3	0.8	0.42	0.68598	45.0
η_4 = 1306, g_4 = 3								
H_2O	rotational[d]	140	0, 0, 0	$8.6(T_0/T)^{1/2} + 0.5$	1	44205	0.14311	69.3
m = 3, η_1 = 3652, g_1 = l	6.3	1600	0, 1, 0	$8.6(T_0/T)^{1/2} + 0.5$	1	41.2	0.09427	56.4
η_1 = 1595, g_2 = l	2.7	3760[a]	0, 2, 0	$8.6(T_0/T)^{1/2} + 0.5$	1	0.19	0.13219	60.0
η_3 = 3756, g_3 =l			1, 0, 0			2.30		
			0, 0, 1			22.40		
	1.87	5350	0, 1, 1	$8.6(T_0/T)^{1/2} + 0.5$	1	3.0	0.08169	43.1
	1.38	7250	1, 0, 1	$8.6(T_0/T)^{1/2} + 0.5$	1	2.5	0.11628	32.0
CO	4.7	2143	1	1.1	0.8	20.9	0.07506	25.5
m = l, η_1 = 2143, g_1 = 1	2.35	4260	2	1.0	0.8	0.14	0.16758	20.0

Sources: Edwards, D. K.: Molecular Gas Band Radiation, in T. F. Irvine, Jr., and J. P. Hartnett (eds.), *Advances in Heat Transfer*, vol. 12, pp. 115–193, Academic Press, New York, 1976; Edwards, D. K., and Balakrishnan, A.: Thermal Radiation by Combustion Gases, *IJHMT*, vol. 16, no. 1, pp. 25–40, 1973.

[a] Upper band limit.

[b] Use values for the 10.4-μm band instead of those for the 9.4-μm band.

[c] See notes in Edwards and Balakrishnan (1973).

[d] For the H_2O rotational band, $\alpha(T) = \alpha_0 \exp[-9.0(T_0/T)^{1/2}], \beta(T_0/T)^{1/2}, \omega_0(T/T_0)^{1/2}$ $a(T)$; if the calculated lower band limit is negative, use $\eta = 0$ for the lower limit (the band width then equals the calculated upper limit); further details are in Modak (1979).

Greif and coworkers [Hsieh and Greif (1972), Lin and Greif (1973, 1974), Hashemi et al. (1976), Chu and Greif (1978)] developed wide-band correlations from basic spectroscopic theory, finding good agreement with experimental measurements in many cases. With this approach, no arbitrary constants are introduced, and recourse to experimental data is not needed to evaluate the constants.

Tien and Lowder (1966) devised the continuous correlation

$$\frac{\bar{A}_l}{\omega} = \ln\left[uf(B)\frac{u+2}{u+2f(B)}+1\right] \tag{A.3}$$

where ω is the bandwidth parameter and $f(B) = 2.94[1 - \exp(-2.60B)]$. This does not satisfy the square-root limit in Equation 9.30 [Cess and Tiwari (1972)], and has been found to be in error for very small values of B. Other correlations have been constructed by Cess and Tiwari:

$$\frac{\bar{A}_l}{\omega} = 2\ln\left[1+\frac{u}{2+u^{1/2}(1+1/B)^{1/2}}\right] \tag{A.4}$$

and Goody and Belton (1967):

$$\frac{\bar{A}_1}{\omega} = 2\ln\left[1+\frac{\sqrt{B}u}{(u+4B)^{1/2}}\right] \tag{A.5}$$

A more complicated expression that covers all ranges is given by Morizumi (1979) who also summarizes some of the other correlations. Tiwari (1976) compares the results of using various narrow-band models in developing the exponential wide-band model. In addition, the correlations outlined above are compared and analyzed for regions of accurate use.

To determine the effect of the band models on the final radiative transfer results, several band models were applied to two problems [Tiwari (1977)] involving radiative transfer in gases with internal heat sources and heat transfer. In most instances good agreement was obtained by using the various models, but it is necessary to examine the reference to appreciate the detailed comparisons. A model to apply the exponential wide-band properties in a multidimensional geometry is in Modest (1983).

EXAMPLE A.1 Find the effective bandwidth $\bar{A}$ of the 9.4-μm band for pure CO_2 at 1 atm and 500K for a path length S of 0.364 m.

To obtain $\bar{A}$ from the relations in Equation A.1, the values of u and B must be determined so the correct relation can be selected. To find $u = X\alpha/\omega$, the values of all three quantities on the right need to be determined using data from Table A.2 and the corresponding relations, and to determine $B = \beta P_e$, values of β and P_e must be found.

To find α, the values of $\Psi(T)$ and $\Psi(T_0)$ must be found using Equation A.2c. For the 9.4 μm band, values from Table A.2 (noting the footnote for this band) are $\alpha_0 = 2.48 \times 10^{-9}$ m^2/g $\cdot$ cm, $\delta_1 = -1$, $\delta_2 = 0$, $\delta_3 = -1$, giving $v_{0,1} = 1$, $v_{0,2} = v_{0,3} = 0\cdot$ Also $g_1 = 1$, $g_2 = 2$, $g_3 = 1$, and $\eta_1 = 1351$cm^{-1}, $\eta_2 = 667$cm^{-1}, and $\eta_3 = 2396$ cm^{-1}. Using $h = 6.626 \times 10^{-34}$ J $\cdot$ s, $k = 1.381 \times 10^{-23}$ J/K, and $c = 2.998 \times 10^{10}$ cm/s gives $\mu_1 = 3.887$, $\mu_2 = 1.919$, and $\mu_3 = 6.893$. The μ_0 values are a factor of 5 larger, respectively. Substituting into Equation A.33c) gives $\Psi(T) = 0.0415$ and $\Psi(T_0) = 7.266 \times 10^{-9}$. Substituting further into Equation A.1a gives $\alpha(T) = 0.01341$ m^2/g $\cdot$ cm.

To find a value for β, values of $\Phi(T)$ and $\Phi(T_0)$ must now be determined. Substituting into Equation (A.2d) results in $\Phi(T)=4.479$ and $\Phi(T_0) = 1.0237$, and from Equation (A.2b), $\beta(T) = 0.04017(100/500)^{1/2}$ (4.479/1.024) = 0.079.

The value of ω is obtained from $\omega = \omega_0(T/T_0)^{1/2}$ using ω_0 from Table A.2 to give $\omega = 10.1(500/100)^{1/2} = 22.58$cm^{-1}.

The mass path length X is defined as ρS, and the value of ρ is found from the ideal gas law as $\rho = PM/RT = 1$ atm x 44 (kg/kg $\cdot$ mol)/[0.08206(atm $\cdot$ m^3/kg $\cdot$ mol $\cdot$ K) $\times$ 500K] = 1.072kg/m^3 = 1.072×10^3g/m^3. Thus, $X = 1.07 \times 10^3$g/m^3 $\times$ 0.364m = 390.3 g/m^2, and $u = X\alpha/\omega = 389.5$ (g/m^2) $\times$ 0.01346 (m^2/g $\cdot$ cm)/22.58 (cm^{-1}) = 0.232.

Now the value of $P_e = [P/P_0 + (p/P_0)(b - 1)]^n$ is found for pure CO_2 at 1 atm using b and n from Table A.2 to give $P_e = (1.3)^{0.8} = 1.234$, so $B = ßP_e = 0.0970$. Examining the relation for $\bar{A}$ (Equations A.1) shows that for $B < 1$ and for u between $B = 0.0970$ and $B^{-1} = 10.309$, which is the case here,

$$\bar{A} = \omega[2(Bu)^{1/2} - B] = 22.58[2(0.0970 \times 0.232)^{1/2} - 0.0970] = 4.58 \text{ cm}^{-1}$$

This compares reasonably well with the experimental value for these conditions of 5.9 cm^{-1} from Edwards (1960). The predictions from other correlations for this band at these conditions are $\bar{A}_{CT}$ = 2.81 (Equation A.4), $\bar{A}_{GB}$ = 3.97 (Equation A.5), and $\bar{A}_{TL}$ = 4.49 (Equation A.3).

Additional complexities are introduced when a gas mixture is considered. For example, the partial pressure *p* of an absorbing gas in a multi-component system varies with *T* and *P*, the populations of the energy states vary with *T*, and the overlapping of spectral lines changes with *P*. It is thus very complex to formulate analytically the dependence of $\bar{A}_l$ on *T*, *p*, and *P* for a real gas mixture. Useful results must depend heavily on experiment while theory is used as a guide. Some calculations for mixtures are in Edwards and Balakrishnan (1973). If two gases are present that both absorb energy, their band absorptivities may overlap in some spectral regions. In this case, Hottel and Sarofim (1967) show that, for two gases *a* and *b* in an overlapping band of width $\Delta\eta$,

$$\bar{A}_{a+b} = \Delta\eta\left[1 - \left(1 - \frac{\bar{A}_a}{\Delta\eta}\right)\left(1 - \frac{\bar{A}_b}{\Delta\eta}\right)\right] = \bar{A}_a + \bar{A}_b - \frac{\bar{A}_a \bar{A}_b}{\Delta\eta} \qquad \text{(A.6)}$$

Thus the simple sum of the two $\bar{A}$ is reduced by the quantity $\bar{A}_a \bar{A}_b / \Delta\eta$ (see also Equations 9.61 and 9.64 of the text). Restriction is to wave number intervals over which both A_a and $\bar{A}_a$ and $\bar{A}_b$, are applicable average values and in which there is no correlation between the positions of the individual spectral lines of gases *a* and *b*.

HOMEWORK

A.1 For a line-width parameter of B = 0.2, prepare a plot comparing various band correlation functions of effective bandwidth to actual bandwidth, $\frac{\bar{A}_\ell}{\omega}$, as a function of the parameter u containing mass path length, for $0.01 \le u \le 100$. Compare the correlation functions of Edwards and Menard (Equation A.1), Tien and Lowder (Equation A.3), Cess and Tiwari (Equation A.4), and Goody and Belton (Equation (A.5).

A.2 Find the effective bandwidth $\bar{A}$ of the 9.4 μm band of CO_2 at a partial pressure of 0.4 atm in a mixture with nitrogen at a total pressure of 1 atm. The gas temperature is 500 K, and the path length S is 0.364 m. Compare with the result in Example A.1.

Answer: 2.09 cm^{-1}.

A.3 For pure CO gas at 1 atm pressure, determine the effective bandwidth for the 4.67 μm spectral band at T = 600 K for a path length of S = 0.5 m.

Answer: 207.3 cm^{-1}.

A.4 From Figure 9.5 of the text, estimate the effective bandwidth for the 2.7 μm CO_2 band at 830 K, 10 atm, and a path length of 38.8 cm. Compare this with the result computed from the correlations in Table A.2.

Answer: 414 cm^{-1}.

REFERENCES:

Aroeste, H. and Benton, W.C.: Emissivity of Hydrogen Atoms at High Temperatures, *J. Appl. Phys.*, vol. 27, pp. 117–121, 1956.

Bond, J. W., Jr., Watson, K. M., and Welch, J. A. Jr.: *Atomic Theory of Gas Dynamics*, Addison-Wesley, Reading, MA, 1965.

Brosmer, M. A., and Tien, C. L.: Thermal Radiation Properties of Acetylene, *JHT*, vol. 107, pp. 943–948, 1985.

Charalampopoulos, T. T., and Felske, J. D.: Total Band Absorptance, Emissivity, and Absorptivity of the Pure Rotational Band of Water Vapor, *JQSRT*, vol. 30, no. 1, pp. 89–96, 1983.

Cess, R. D., and Tiwari, S. N.: Infrared Radiative Energy Transfer in Gases, in T. F. Irvine, Jr., and J. P. Hartnett (eds.), *Advances in Heat Transfer*, vol. 8, pp. 229–283, Academic Press, New York, 1972

Chan, S. H., and Tien, C. L.: Infrared Radiation Properties of Sulfur Dioxide, *JHT*, vol. 93, no. 2, pp. 172–178, 1971.

Chu, K. H., and Greif, R.: Theoretical Determination of Band Absorption for Nonrigid Rotation with Applications to CO, NO, N_2O and CO_2, *JHT*, vol. 100, pp. 230–234, 1978.

Denison, M. K., and Webb, B. W.: A Spectral Line-Based Weighted-Sum-of-Gray-Gases Model for Arbitrary RTE Solvers, *JHT*, vol. 115, no. 4, pp. 1004–1012, 1993.

Denison, M. K., and Webb, B. W.: The Spectral-Line Weighted-Sum-of-Gray-Gases Model for H_2O/CO_2 Mixtures, *JHT*, vol. 117, pp. 788–798, 1995.

Domoto, G. A.: Frequency Integration for Radiative Transfer Problems Involving Homogeneous Non-Gray Gases: The Inverse Transmission Function, *JQSRT*, vol. 14, pp. 935–942, 1974.

Edwards, D. K.: Absorption of Infrared Bands of Carbon Dioxide Gas at Elevated Pressures and Temperatures, *JOSA*, vol. 50, no. 6, pp. 617–626, 1960.

Edwards, D. K.: Radiant Interchange in a Nongray Enclosure Containing an Isothermal Carbon Dioxide–Nitrogen Gas Mixture, *JHT*, vol. 84, no. 1, pp. 1–11, 1962.

Edwards, D. K.: Absorption of Radiation by Carbon Monoxide Gas According to the Exponential Wide-Band Model, *Appl. Opt.*, vol. 4, no. 10, pp. 1352–1353, 1965.

Edwards, D. K.: Molecular Gas Band Radiation, in T. F. Irvine, Jr., and J. P. Hartnett (eds.), *Advances in Heat Transfer*, vol. 12, pp. 115–193, Academic Press, New York, 1976.

Edwards, D. K., and Menard, W. A.: Comparison of Models for Correlation of Total Band Absorption, *Appl. Opt.*, vol. 3, no. 5, pp. 621–625, 1964a.

Edwards, D. K., and Menard, W. A.: Correlations for Absorption by Methane and Carbon Dioxide Gases, *Appl. Opt.*, vol. 3, no. 7, pp. 847–852, 1964b.

Edwards, D. K., and Nelson, K. E.: Rapid Calculation of Radiant Energy Transfer between Nongray Walls and Isothermal H_2O or CO_2 Gas, *JHT*, vol. 84, no. 4, pp. 273–278, 1962.

Edwards, D. K., and Sun, W.: Correlations for Absorption by the 9.4-μ and 10.4- μ CO_2 Bands, *Appl. Opt.*, vol. 3, no. 12, pp. 1501–1502, 1964.

Edwards, D. K., Flornes, B. J., Glassen, L. K., and Sun, W.: Correlation of Absorption by Water Vapor at Temperatures from 300 K to 1100 K, *Appl. Opt.*, vol. 4, no. 6, pp. 715–721, 1965.

Edwards, D. K., Glassen, L. K., Hauser, W. C., and Tuchscher, J. S.: Radiation Heat Transfer in Nonisothermal Nongray Gases, *JHT*, vol. 89, no. 3, pp. 219–229, 1967.

Edwards, D. K., and Balakrishnan, A.: Thermal Radiation by Combustion Gases, *IJHMT*, vol. 16, no. 1, pp. 25–40, 1973.

Felske, J. D., and Tien, C. L.: A Theoretical Closed-Form Expression for the Total Band Absorptance of Infrared–Radiating Gases, *IJHMT*, vol. 17, pp. 155–158, 1974

Goody, R. M., and Belton, M. J. S.: Radiative Relaxation Times for Mars (Discussion of Martian Atmospheric Dynamics), *Planet. Space Sci.*, vol. 15, no. 2, pp. 247–256, 1967.

Hashemi, A., Hsieh, T. C., and Greif R.: Theoretical Determination of Band Absorption with Specific Application to Carbon Monoxide and Nitric Oxide, *JHT*, vol. 98, pp. 432–437, 1976.

Hines, W. S., and Edwards, D. K.: Infrared Absorptivities of Mixtures of Carbon Dioxide and Water Vapor, *Chem. Eng. Prog. Symp. Ser.*, vol. 64, no. 82, pp. 173–180, 1968.

Hottel, H. C, and Sarofim, A. F.: *Radiative Transfer*, McGraw–Hill, New York, 1967.

Hsieh, T. C, and Greif, R.: Theoretical Determination of the Absorption Coefficient and the Total Band Absorptance Including a Specific Application to Carbon Monoxide, *IJHMT*, vol. 15, pp. 1477–1487, 1972.

Jones, M. C.: Far Infrared Absorption in Liquefied Gases, NBS Technical Note 390, National Bureau of Standards, Boulder, CO, 1970.

Kamiuto, K., and Tokita, Y.: Wideband Spectral Models for the Absorption Coefficient of Water Vapor, *JTHT*, vol. 8, no. 4, pp. 808–810, 1994.

Kunitomo, T., Masuzaki, H., Ueoka, S., and Osumi, M.: Experimental Studies of the Properties of Sulfur Dioxide, *JQSRT*, vol. 25, pp. 345–349, 1981.

Lin, J. C., and Greif, R.: Total Band Absorptance of Carbon Dioxide and Water Vapor Including Effects of Overlapping, *IJHMT*, vol. 17, pp. 793–795, 1974.

Marin, O., and Buckius, R.: A Simplified Wide Band Model of the Cumulative Distribution Function for Water Vapor, *IJHMT*, vol. 41, pp. 2877–2892, 1998a.

Marin, O., and Buckius, R.: A Simplified Wide Band Model of the Cumulative Distribution Function for Carbon Dioxide, *IJHMT*, vol. 41, pp. 3881–3897, 1998b.

Modest, M. F.: Evaluation of Spectrally–Integrated Radiative Fluxes of Molecular Gases in Multi-dimensional Media, *IJHMT*, vol. 26, no. 10, pp. 1533–1546, 1983.

Morizumi, S. J.: Comparison of Analytical Model with Approximate Models for Total Band Absorption and Its Derivative, *JQSRT*, vol. 22, no. 5, pp. 467–474, 1979.

Novotny, J. L., Negrelli, D. E., and Van der Driessche, T.: Total Band Absorption Models for Absorbing-Emitting Liquids: CCl_4, *JHT*, vol. 96, pp. 27–31, 1974.

Solovjov, V. P., and Webb, B. W.: Radiative Transfer Model Parameters for Carbon Monoxide at High Temperature, in J. S. Lee (ed.), *Heat Transfer*—1998, *Proc. 11th Int. Heat Transfer Conf*, KyongJu, Korea, vol. 7, pp. 445–450, Taylor & Francis, New York, 1998.

Stull, V. R., and Plass, G. N.: Emissivity of Dispersed Carbon Particles, *JOSA*, vol. 50, no. 2, pp. 121–129, 1960.

Tien, C. L.: Band and Total Emissivity of Ammonia, *IJHMT*, vol. 16, pp. 856–857, 1973.

Tien, C. L., and Lowder, J. E.: A Correlation for Total Band Absorptance of Radiating Gases, *IJHMT*, vol. 9, no. 7, pp. 698–701, 1966.

Tiwari, S. N.: Band Models and Correlations for Infrared Radiation, in *Radiative Transfer and Thermal Control*, vol. 49 of *Progress in Astronautics and Aeronautics Series*, pp. 155–182, AIAA, 1976.

Tiwari, S. N.: Applications of Infrared Band Model Correlations to Nongray Radiation, *IJHMT*, vol. 20, no. 7, pp. 741–751, 1977.

Tuntomo, A., Park, S. H., and Tien, C. L.: Infrared Radiation Properties of Ethylene, *Exp. Heat Transfer*, vol. 2, pp. 91–103, 1989.

Weiner, M. M.: Radiant Heat Transfer in Non-isothermal Gases, Ph.D. thesis, University of California at Los Angeles, 1966.

Appendix B: Derivation of Geometric Mean Beam Length Relations

The Geometric Mean Beam Lengths depend on both geometry and wavelength through the definitions

$$A_j F_{j-k} \overline{t}_{\lambda,j-k} = \int_{A_k} \int_{A_j} \frac{e^{-\kappa_\lambda S} \cos\theta_k \cos\theta_j}{\pi S^2} dA_j \, dA_k \tag{B.1}$$

$$A_j F_{j-k} \overline{\alpha}_{\lambda,j-k} = A_j F_{j-k} \left(1 - \overline{t}_{\lambda,j-k}\right) \tag{B.2}$$

The double integral in Equation B.1 must be evaluated for various orientations of surfaces A_j and A_k; the result will depend on k_λ. Derivations for some specific geometries are now considered.

B.1 Hemisphere to Differential Area at Center of its Base

Let A_j be the surface of a hemisphere of radius R, and dA_k be a differential area at the center of the base (Figure B.1). Then Equation B.1 becomes, since $S=R$ and $\theta_i = 0$,

$$A_j dF_{j-dk} \overline{t}_{\lambda,j-dk} = dA_k \int_{A_j} \frac{e^{-\kappa_\lambda R} \cos\theta_k \cos(0)}{\pi R^2} dA_j$$

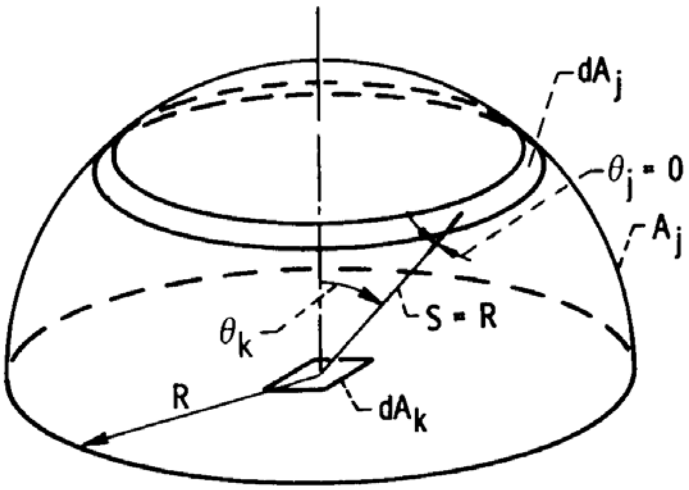

FIGURE B.1 Hemisphere filled with isothermal medium.

The convenient dA_j is a ring element $dA_j = 2\pi R^2 \sin\theta_k \, d\theta_k$, and the factors involving R can be taken out of the integral. This gives

$$A_j dF_{j-dk} \overline{t}_{\lambda,j-dk} = dA_k \int_{A_j} \frac{e^{-\kappa_\lambda R} 2\pi R^2}{\pi R^2} \int_{\theta_k=0}^{\pi/2} \cos\theta_k \sin\theta_k \, d\theta_k = dA_k e^{-\kappa_\lambda R}$$

With $A_j \, dF_{j-dk} = dA_k \, F_{dk-j}$ and $F_{dk-j} = 1,$, this reduces to

$$\overline{t}_{\lambda,j-dk} = e^{-\kappa_\lambda R} \tag{B.3}$$

This especially simple relation is used later in the concept of mean beam length where radiation from an actual volume of a medium is replaced by that from an equivalent hemisphere.

B.2 Top of Right Circular Cylinder to Center of its Base

This geometry is in Figure B.2. Since $\theta_j = \theta_k = \theta$, the integral in Equation B.1 becomes, for the top of the cylinder A_j radiating to the element dA_k at the center of its base,

$$A_j dF_{j-dk} \overline{t}_{\lambda, j-dk} = dA_k \int_{A_j} \frac{e^{-\kappa_\lambda S} \cos^2 \theta}{\pi S^2} dA_j \tag{B.4}$$

Since $\xi^2 = S^2 - h^2, dA_j = 2\pi\xi \; d\xi = 2\pi S \; dS.$ Then, using cos θ = *h/S*,

$$A_j \; dF_{j-dk} \overline{t}_{\lambda, j-dk} = dA_k \, 2h^2 \int_h^{\sqrt{R^2+h^2}} \frac{e^{-\kappa_\lambda S}}{S^3} dS \tag{B.5}$$

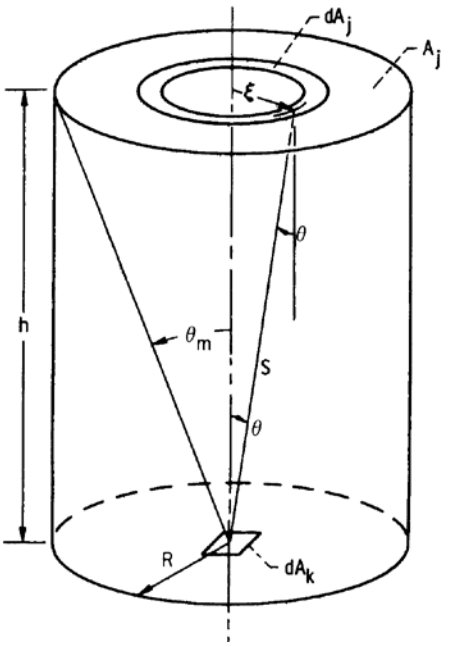

FIGURE B.2 Geometry for exchange from top of gas-filled cylinder to center of its base.

Now let $\kappa_\lambda S = \tau_\lambda$ to obtain

$$A_j \; dF_{j-dk} \overline{t}_{\lambda, j-dk} = dA_k \, 2h^2 \kappa_\lambda^2 \int_{\tau_\lambda = \kappa_\lambda h}^{\kappa_\lambda \sqrt{R^2+h^2}} \frac{e^{-\tau_\lambda}}{\tau_\lambda^3} d\tau_\lambda \tag{B.6}$$

This integral can be expressed in terms of the exponential integral function defined in Appendix D of the text, by writing

$$\int_{\tau_\lambda = \kappa_\lambda h}^{\kappa_\lambda \sqrt{R^2+h^2}} \frac{e^{-\tau_\lambda}}{\tau_\lambda^3} d\tau_\lambda = \int_{\tau_\lambda = \infty}^{\kappa_\lambda \sqrt{R^2+h^2}} \frac{e^{-\tau_\lambda}}{\tau_\lambda^3} d\tau_\lambda - \int_{\tau_\lambda = \infty}^{a_\lambda h} \frac{e^{-\tau_\lambda}}{\tau_\lambda^3} d\tau_\lambda \tag{B.7}$$

Letting $\tau_\lambda = \left(\kappa_\lambda \sqrt{R^2+h^2}\right)\Big/\mu$ and $\kappa_\lambda h/\mu$, respectively, in the two integrals gives

$$-\frac{1}{\left(\kappa_\lambda \sqrt{R^2+h^2}\right)^2}\int_0^1 \mu e^{-\kappa_\lambda \sqrt{R^2+h^2}/\mu} d\mu + \frac{1}{\left(\kappa_\lambda h\right)^2}\int_0^1 \mu e^{-\kappa_\lambda h/\mu} d\mu$$

The integral in Equation B.6 is then written in terms of the exponential integral function as

$$\int_{\tau_\lambda=\kappa_\lambda h}^{\kappa_\lambda\sqrt{R^2+h^2}} \frac{e^{-\tau_\lambda}}{\tau_\lambda^3} d\tau_\lambda = \frac{1}{\left(\kappa_\lambda h\right)^2} E_3\left(\kappa_\lambda h\right) - \frac{1}{\left[\kappa_\lambda h\sqrt{(R/h)^2+1}\right]^2} E_3\left[\kappa_\lambda h\sqrt{\left(\frac{R}{h}\right)^2+1}\right] \qquad \text{(B.8)}$$

so it can be readily evaluated for various values of the parameters R/h and $\kappa_\lambda h$.

B.3 Side of Cylinder to Center of its Base

Let dA_j be a ring around the wall of a cylinder as in Figure B.3, and note that $dA_j = 2\pi R dz$, $\cos\theta_k = z/S$, $\cos\theta_j = R/S$, and $z\,dz = S dS$. Then Equation B.1 is written for the side of the cylinder to dA_k as

$$A_j dF_{j-dk}\overline{\tau}_{\lambda,j-dk} = 2dA_k R^2 \int_R^{\sqrt{R^2+h^2}} \frac{e^{-a_\lambda S}}{S^3} dS \qquad \text{(B.9)}$$

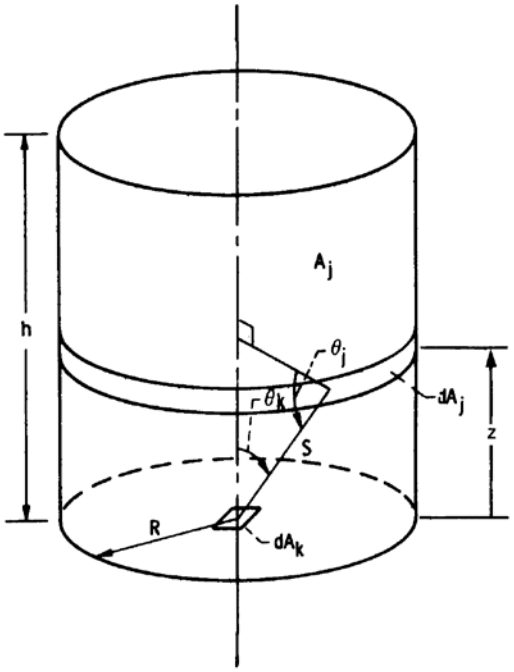

FIGURE B.3 Geometry for exchange from side of gas-filled cylinder to center of its base.

This is of the same form as Equation B.5, and gives the result

$$A_j dF_{j-dk}\,\bar{t}_{\lambda,\,j-dk}$$

$$= 2dA_k \left(\frac{R}{h}\right)^2 (\kappa_\lambda h)^2 \left\{ \frac{1}{\left[\kappa_\lambda h \left(R/h\right)^2\right]} E_3\left[\kappa_\lambda h\left(\frac{R}{h}\right)\right] - \frac{1}{\left[\kappa_\lambda h\sqrt{(R/h)^2+1}\right]^2} E_3\left[\kappa_\lambda h\sqrt{\left(\frac{R}{h}\right)^2+1}\right] \right\} \tag{B.10}$$

As for Equation B.8, this is readily evaluated for various values of R/h and $\kappa_\lambda h$.

B.4 Entire Sphere to Any Area on its Surface or to its Entire Surface

From Figure B.4, since $\theta_k = \theta_j$ let them be simply θ; then $S = 2R\cos\theta$. Starting with Equation B.4, $dA_j \cos\theta/S^2$ is the solid angle by which dA_j is viewed from dA_k. The intersection of the solid angle with a unit hemisphere shows that this equals $2\pi \sin\theta\, d\theta$. Then

$$A_j\, dF_{j-dk}\,\bar{t}_{\lambda,\,j-dk} = dA_k \int_{\theta=0}^{\pi/2} e^{-\kappa_\lambda S}\, 2\cos\theta \sin\theta d\theta = \frac{2dA_k}{4R^2}\int_{S=0}^{2R} e^{-\kappa_\lambda S} S dS$$

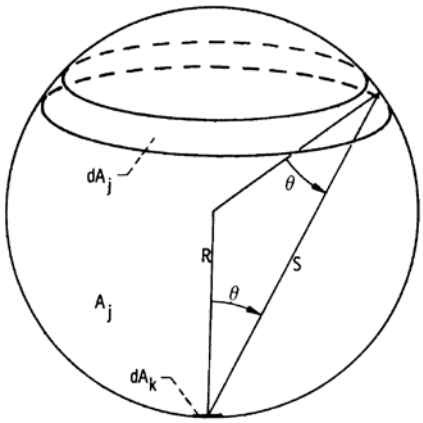

FIGURE B.4 Geometry for exchange from surface of gas-filled sphere to itself.

Integrating gives

$$A_j\, dF_{j-dk}\,\bar{t}_{\lambda,\,j-dk} = \frac{2dA_k}{(2a_\lambda R)^2}\left[1-\left(2\kappa_\lambda R+1\right)e^{-2\kappa_\lambda R}\right] \tag{B.11}$$

which has a single parameter $2\kappa_\lambda R$, the sphere optical diameter.

Equation B.11 is integrated over any finite area A_k to give $\bar{t}_\lambda$ from the entire sphere to A_k as $A_j F_{j-k}\,\bar{t}_{\lambda,\,j-k} = \left[2A_k/\left(2\kappa_\lambda R\right)^2\right]\left[1-\left(2\kappa_\lambda R+1\right)e^{-2\kappa_\lambda R}\right]$. Since $F_{j-k} = A_k/A_j$, from Equation 4.17,

$$\bar{t}_{\lambda,\,j-k} = \frac{2}{(2\kappa_\lambda R)^2}\left[1-\left(2\kappa_\lambda R+1\right)e^{-2\kappa_\lambda R}\right] \tag{B.12}$$

which also applies for the entire sphere to its entire surface.

B.5 Infinite Plate to Any Area on Parallel Plate

In Figure B.5 consider on one plate an element dA_k, and on the other plate a concentric ring element dA_j centered about the normal to dA_k. The geometry is like that in Figure B.2 for a ring on the top of a cylinder to the center of its base. Then, from Equation B.6,

$$A_j\, dF_{j-dk}\, \overline{t}_{\lambda, j-dk} = dA_k\, 2(\kappa_\lambda D)^2 \int_{\tau_\lambda=\kappa_\lambda D}^{\infty} \frac{e^{-\tau_\lambda}}{\tau_\lambda^3}\, d\tau_\lambda$$

where $\kappa_\lambda D$ is the optical spacing between the plates. By using the procedure leading to Equation B.8, the integral is transformed to $E_3(\kappa_\lambda D)/(\kappa_\lambda D)^2$. Then integrating over any finite area A_k as in Figure B.5 gives $A_j F_{j-k}\, \overline{t}_{\lambda, j-k} = A_k\, 2E_3(\kappa_\lambda D)$. With $A_j F_{j-k} = A_k F_{k-j}$ and $F_{k-j} = 1$, this reduces to

$$\overline{t}_{\lambda, j-k} = 2E_3(\kappa_\lambda D) \tag{B.13}$$

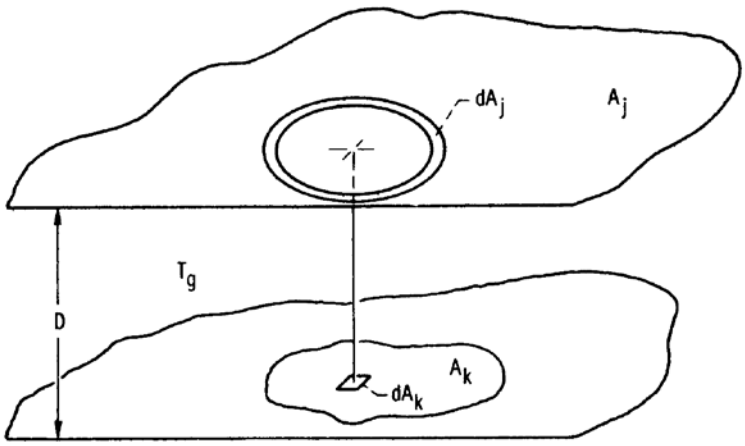

FIGURE B.5 Isothermal layer of medium between infinite parallel plates.

B.6 Rectangle to a Directly Opposed Parallel Rectangle

Consider, as in Figure B.6, the exchange from a rectangle to an area element on a directly opposed parallel rectangle. The upper rectangle is divided into a circular region and a series of partial rings of small width. The contribution from the circle of radius R to $A_j dF_{j-dk}\, \overline{t}_{\lambda, j-dk}$ can be found from Equations B.6 and B.8, for the top of a cylinder to the center of its base. For the nth partial ring, let f_n be the fraction it occupies of a full circular ring. Then, by use of Equation B.4, the contribution of all the partial rings to $A_j dF_{j-dk}\, \overline{t}_{\lambda, j-dk}$ is approximated by

$$dA_k \sum_m f_n \frac{e^{-\kappa_\lambda S_n}}{\pi S_n^2} \left(\frac{D}{S_n}\right)^2 2\pi R_n \Delta R_n = dA_k\, 2D^2 \sum_n f_n \frac{e^{-\kappa_\lambda S_n}}{\left(D^2 + R_n^2\right)} R_n \Delta R_n$$

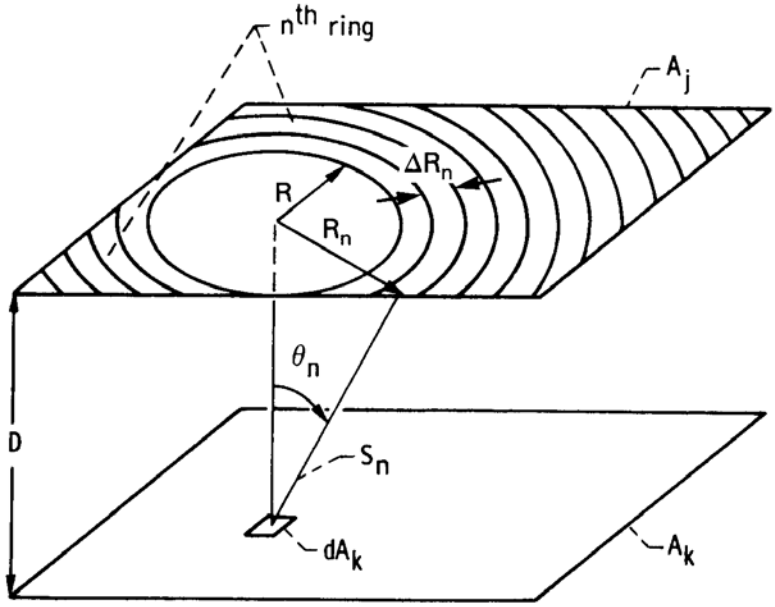

FIGURE B.6 Geometry for exchange between two directly opposed parallel rectangles with intervening translucent medium.

This evaluation of $A_j dF_{j-dk}\overline{t}_{\lambda,j-dk}$ is carried out for several area patches on A_k. This is usually sufficient, so the integration over A_k can be performed as indicated by Equation B.1 to yield

$$A_j F_{j-k}\overline{t}_{\lambda,j-k} = \int_{A_k} A_j dF_{j-dk}\overline{t}_{\lambda,j-dk}$$

EXAMPLE B.1 A nongray, absorbing-emitting plane layer with κ_λ as in Figure B.7 is 1.2 cm thick and is on top of an opaque diffuse-gray infinite plate. The plate temperature has been raised suddenly, so the layer is still at its initial uniform temperature. What is the net heat flux being lost from the plate-layer system? Neglect heat conduction effects in the layer, and neglect any reflections at the upper boundary of the layer.

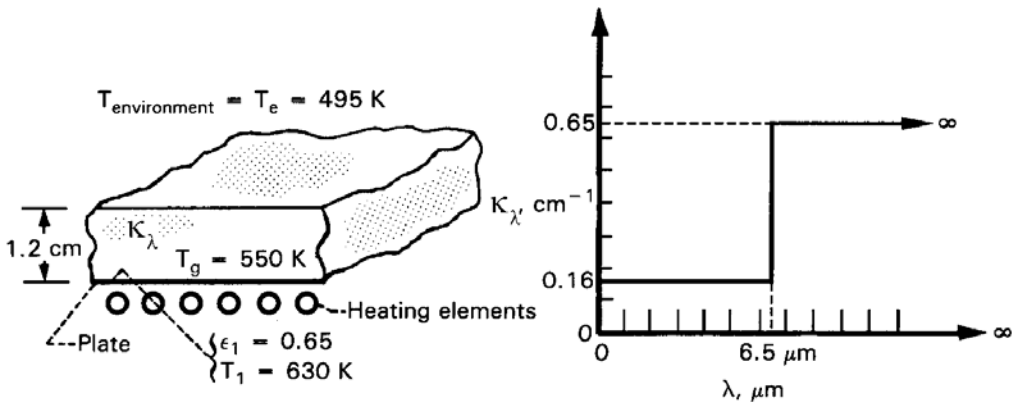

FIGURE B.7 Plane layer of nongray absorbing-emitting material.

The uniform environment above the layer acts as a black enclosure at T_e. Equation 10.79b of the text can be applied directly by integrating in two spectral bands and using $\epsilon_{\lambda 2} = 1$. The geometric-mean transmittance factors are obtained from

Equation B.13 as $\bar{t}_{\lambda,1} = 2E_3(0.16\times1.2) = 0.7142, \quad 0 \le \lambda \le 6.5\mu\text{m}; \; \bar{t}_{\lambda,2} = 2E_3(0.65\times1.2) = 0.2974, \quad 6.5\mu\text{m} \le \lambda \le \infty$. This yields

$$\begin{aligned} q = -q_2 &= \epsilon_1 \bar{t}_{\lambda,1}(\sigma T_1^4 F_{0\to6.5T_1} - \sigma T_e^4 F_{0\to6.5T_e}) \\ &+ (1-\bar{t}_{\lambda,1})[1+(1-\epsilon_1)\bar{t}_{\lambda,1}](\sigma T_g^4 F_{0\to6.5T_g} - \sigma T_e^4 F_{0\to6.5T_e}) \\ &+ \epsilon_1 \bar{t}_{\lambda,2}[\sigma T_1^4 (1-F_{0\to6.5T_1}) - \sigma T_e^4 (1-F_{0\to6.5T_e}) \\ &+ (1-\bar{t}_{\lambda,2})[1+(1-\epsilon_1)\bar{t}_{\lambda,2}][\sigma T_g^4 (1-F_{0\to6.5T_g}) - \sigma T_e^4 (1-F_{0\to6.5T_e})] \end{aligned}$$

Inserting the values $F_{0\to6.5\times630}$ = 0.4978, $F_{0\to6.5\times550}$ = 0.3985 and $F_{0\to6.5\times495}$ = 0.3220 yields q = 2954 W/m^2.

B.7 Geometric-Mean Beam Length for Spectral Band Enclosure Equations

For use in the spectral band enclosure Equation 10.84 in the text, the absorption integral in Equation 10.89 must be evaluated between pairs of enclosure surfaces for the wavelength bands involved. When more than a few bands absorb appreciably, the enclosure solution requires considerable computational effort. A simplification was developed by Dunkle (1964) by assuming that the integrated band absorption $\bar{\alpha}_l(S)$ is a *linear function* of path length. This has some physical basis, as it holds exactly for a band of weak nonoverlapping lines (Equation 9.16 in the text). Also, it is the form of some of the effective bandwidths in the exponential wide band correlations of on-line Appendix A (Equation A.1 at **http://www.thermalradiation.net/**). As shown in Dunkle by means of a few examples, reasonable values for the energy exchange are obtained using this approximation. Hence, let κ_l in Equation 10.90 have the linear form from Equation 9.27 (note that the bandwidth $\Delta\lambda_l = \omega$ in Equation 9.27)

$$\bar{\alpha}_l(S) = \frac{\bar{A}_l(S)}{\Delta\lambda_l} = \frac{\bar{A}_l(S)}{\omega} = \frac{\bar{A}_l(S)}{m\delta} = \frac{S_c}{\delta} S \tag{B.14}$$

where S_c and δ are the line intensity and the spacing of the individual weak spectral lines, as in Chapter 9 of the text.

Now define a mean path length $\bar{S}_{k-j}$ called the *geometric-mean beam length*, such that α_l evaluated from Equation B.14 by using $S = \bar{S}_{k-j}$ will equal $\bar{\alpha}_{l,k-j}$ from the integral in Equation 10.89 of the text. After substituting $\bar{\alpha}_{l,k-j} = (S_c/\delta)\bar{S}_{k-j}$ and $\alpha_l = (S_c/\delta)S$ into Equation 10.89, the relation for $\bar{S}_{k-j}$ is

$$\bar{S}_{k-j} = \bar{S}_{j-k} = \frac{1}{A_k F_{k-j}} \int_{A_j}\int_{A_k} \frac{\cos\theta_j \cos\theta_k}{\pi S} dA_k dA_j \tag{B.15}$$

which depends only on geometry. This integral is also obtained in Equation B.1 when $\kappa_\lambda S$ is small (optically thin limit). In Dunkle, S_{k-j} values are tabulated for parallel equal rectangles, for rectangles at right angles, and for a differential sphere and a rectangle. Analytical relations for rectangles are in Equations B.16*a*,*b*. For directly opposed parallel equal rectangles with sides of length *a* and *b* and spaced a distance *c* apart,

$$\frac{\bar{S}_{k-j}A_kF_{k-j}}{abc}=\frac{4}{\pi}\left\{\tan^{-1}\frac{\eta\beta}{\xi}+\frac{1}{\eta}\ln\left[\frac{\beta+\xi}{\sqrt{1+\eta^2}\,(\beta+\sqrt{1+\beta^2}}\right]+\frac{1}{\beta}\ln\left[\frac{\eta+\xi}{\sqrt{1+\beta^2}\,(\eta+\sqrt{1+\eta^2})}\right]\right.$$
$$\left.+\frac{1}{\eta\beta}\left[\sqrt{1+\eta^2}+\sqrt{1+\beta^2}-1-\xi\right]\right\} \qquad \text{(B.16}a\text{)}$$

where $\eta = a/c$, $\beta = b/c$ and $\xi=\sqrt{1+\eta^2+\beta^2}$. The F_{k-j} can be obtained from Factor 4 in Appendix C of the text. For rectangles *ab* and *bc* at right angles with a common edge *b*,

$$\frac{\bar{S}_{k-j}A_kF_{k-j}}{abc}=\frac{1}{\pi}\left\{\frac{\gamma}{\alpha}\ln\frac{(1+\sqrt{1+\gamma^2})\sqrt{\alpha^2+\gamma^2}}{\gamma(1+\sqrt{1+\alpha^2+\gamma^2}}+\frac{\alpha}{\gamma}\ln\frac{(1+\sqrt{1+\alpha^2})\sqrt{\alpha^2+\gamma^2}}{\alpha(1+\sqrt{1+\alpha^2+\gamma^2})}\right.$$
$$+\frac{1}{3\gamma\alpha}[(1+\gamma^2)^{3/2}+(1+\alpha^2)^{3/2}+(\alpha^2+\gamma^2)^{3/2}-(1+\alpha^2+\gamma^2)^{3/2}]$$
$$+\frac{\alpha}{\gamma}[\sqrt{1+\alpha^2+\gamma^2}-\sqrt{\alpha^2+\gamma^2}-\sqrt{1+\alpha^2}]$$
$$\left.+\frac{\gamma}{\alpha}[\sqrt{1+\alpha^2+\gamma^2}-\sqrt{\alpha^2+\gamma^2}-\sqrt{1+\gamma^2}]+\frac{2}{3}\left[\frac{\gamma^2}{\alpha}+\frac{\alpha^2}{\gamma}-\frac{1}{2\gamma\alpha}\right]\right\} \qquad \text{(B.16}b\text{)}$$

where α = *a/b* and γ = *c/b*. The F_{k-j} is obtained from Factor 8 in Appendix C of the text. Results for equal opposed parallel rectangles are in Figure B.8, and values for equal parallel rectangles and for rectangles at right angles are in Tables B.1 and B.2. Other $\bar{S}_{k-j}$ values are referenced by Hottel and Sarofim (1967). In Anderson and Hadvig (1989), values are obtained for a medium in the space between two infinitely long coaxial cylinders.

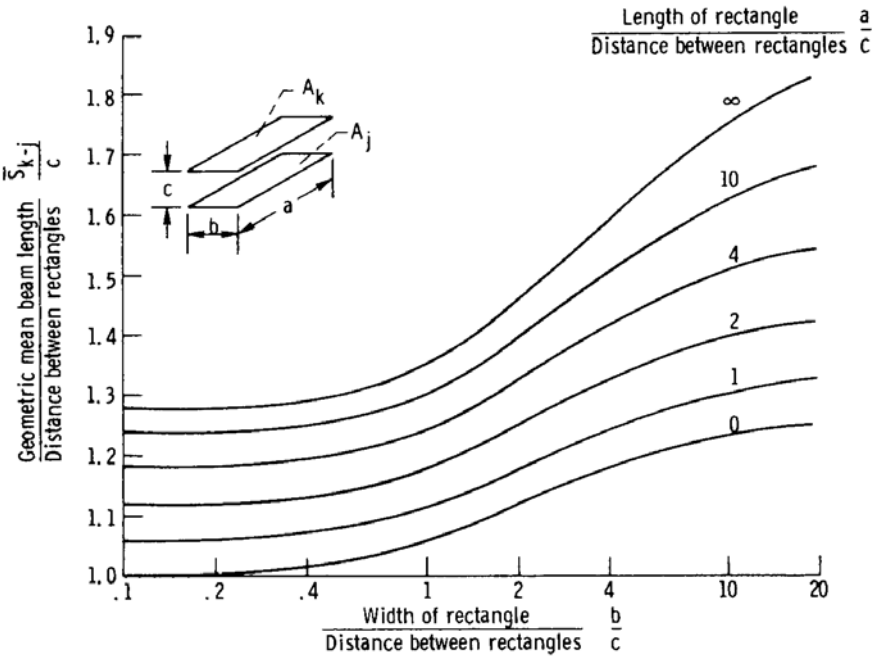

FIGURE B.8 Geometric mean beam lengths for equal parallel rectangles [Dunkle (1964)].

B. Geometric Mean Beam Lengths

For a medium at uniform conditions, the geometric-mean beam length can be used in the effective-bandwidth correlations in on-line Appendix A (**http://www.thermalradiation.net**) to obtain $\bar{A}_l(\bar{S})$. Using $\Delta\lambda_l$ obtained in the next paragraph yields $\bar{\alpha}_l\left(\bar{S}\right) = \bar{A}_l\left(S\right)/\Delta\lambda_l$ from Equation 10.91 of the text and $\bar{t}_l$ from $1-\bar{\alpha}_l$. Then Equations 10.84 and 10.85 of the text can be solved for $q_{l,k}$ for each wavelength band l. The total energies at each surface k are found from a summation over all bands

$$q_k = \sum_{\substack{\text{absorbing}\\ \text{bands}}} q_{l,k}\Delta\lambda_l + \sum_{\substack{\text{nonabsorbing}\\ \text{bands}}} q_{l,k}\Delta\lambda_l \tag{B.17}$$

The wavelength span $\Delta\lambda_l$ of each band is needed to carry out the solution. This span can increase with path length. Edwards and coworkers [Edwards and Nelson (1962), Edwards (1962), Edwards et al. (1967)] give recommended spans for CO_2 and H_2O vapor; these values, in wave number units, are in Table A.3 for the parallel-plate geometry. For other geometries, Edwards and Nelson give methods for choosing approximate spans for CO_2 and H_2O bands. Briefly, the method is to use approximate band spans based on the longest important mass path length in the geometry being studied. With this in mind, the limits of Table B.3 are probably adequate for problems involving CO_2 and H_2O vapor.

If all surface temperatures are specified in a problem, the results from Equation B.17 complete the solution. If q_k is specified for n surfaces and T_k for the remaining $N–n$ surfaces, then the n unknown surface temperatures are guessed, the equations are solved for all q, and then the calculated q_k are compared to the specified values. If they do not agree, new values of T_k for the n surfaces are assumed and the calculation is repeated until the given and calculated q_k agree for all A_k with specified q_k. Equation 11.8, expressed as a sum over the wavelength bands, gives the required energy input to the medium for the specified T_g.

TABLE B.1 Geometric mean beam-length ratios and configuration factors for parallel equal rectangles [Dunkle (1964)]

		c/b										
a/c		0	0.1	0.2	0.4	0.6	1.0	2.0	4.0	6.0	10.0	20.0
0	$\overline{S}_{k-j}/c$	1.000	1.001	1.003	1.012	1.025	1.055	1.116	1.178	1.205	1.230	1.251
	F_{k-j}											
0.1	$\overline{S}_{k-j}/c$	1.001	1.002	1.004	1.013	1.026	1.056	1.117	1.179	1.207	1.233	1.254
	F_{k-j}		0.00316	0.00626	0.01207	0.01715	0.02492	0.03514	0.04210	0.04463	0.04671	0.04829
0.2	$\overline{S}_{k-j}/c$	1.003	1.004	1.006	1.015	1.028	1.058	1.120	1.182	1.210	1.235	1.256
	F_{k-j}		0.00626	0.01240	0.02391	0.03398	0.04941	0.06971	0.08353	0.08859	0.09271	0.09586
0.4	$\overline{S}_{k-j}/c$	1.012	1.013	1.015	1.024	1.037	1.067	1.129	1.192	1.220	1.245	1.267
	F_{k-j}		0.01207	0.02391	0.04614	0.06560	0.09554	0.13513	0.16219	0.17209	0.18021	0.18638
0.6	$\overline{S}_{k-j}/c$	1.025	1.026	1.028	1.037	1.050	1.080	1.143	1.206	1.235	1.261	1.282
	F_{k-j}		0.01715	0.03398	0.06560	0.09336	0.13627	0.19341	0.23271	0.24712	0.25896	0.26795
1.0	$\overline{S}_{k-j}/c$	1.055	1.056	1.058	1.067	1.080	1.110	1.175	1.242	1.272	1.300	1.324
	F_{k-j}		0.02492	0.04941	0.09554	0.13627	0.19982	0.28588	0.34596	0.36813	0.38638	0.40026
2.0	$\overline{S}_{k-j}/c$	1.116	1.117	1.120	1.129	1.143	1.175	1.246	1.323	1.359	1.393	1.421
	F_{k-j}		0.03514	0.06971	0.13513	0.19341	0.28588	0.41525	0.50899	0.54421	0.57338	0.59563
4.0	$\overline{S}_{k-j}/c$	1.178	1.179	1.182	1.192	1.206	1.242	1.323	1.416	1.461	1.505	1.543
	F_{k-j}		0.04210	0.08353	0.16219	0.23271	0.34596	0.50899	0.63204	0.67954	0.71933	0.74990
6.0	$\overline{S}_{k-j}/c$	1.205	1.207	1.210	1.220	1.235	1.272	1.359	1.461	1.513	1.564	1.609
	F_{k-j}		0.04463	0.08859	0.17209	0.24712	0.36813	0.54421	0.67954	0.73258	0.77741	0.81204
10.0	$\overline{S}_{k-j}/c$	1.230	1.233	1.235	1.245	1.261	1.300	1.393	1.505	1.564	1.624	1.680

	F_{k-j}		0.04671	0.09271	0.18021	0.25896	0.38638	0.57338	0.71933	0.77741	0.82699	0.86563
20.0	$\overline{S}_{k-j}/c$	1.251	1.254	1.256	1.267	1.282	1.324	1.421	1.543	1.609	1.680	1.748
	F_{k-j}		0.04829	0.09586	0.18638	0.26795	0.40026	0.59563	0.74990	0.81204	0.86563	0.90785
	$\overline{S}_{k-j}/c$	1.272	1.274	1.277	1.289	1.306	1.349	1.452	1.584	1.660	1.745	1.832
	F_{k-j}		0.04988	0.09902	0.19258	0.27698	0.41421	0.61803	0.78078	0.84713	0.90499	0.95125

TABLE B.2 Configuration factors and mean beam-length functions for rectangles at right angles [Dunkle (1964)]

		c/b											
a/b		0.05	0.10	0.20	0.4	0.6	1.0	2.0	4.0	6.0	10.0	20.0	∞
0.02	A_kF_{k-j}/b^2	0.007982	0.008875	0.009323	0.009545	0.009589	0.009628	0.009648	0.009653	0.009655	0.009655	0.009655	0.009655
	$A_kF_{k-j}\overline{S}_{k-j}/abc$	0.17840	0.12903	0.08298	0.04995	0.03587	0.02291	0.01263	0.006364	0.004288	0.002594	0.001305	
0.05	A_kF_{k-j}/b^2	0.014269	0.018601	0.02117	0.02243	0.02279	0.02304	0.02316	0.02320	0.02321	0.02321	0.02321	0.02321
	$A_kF_{k-j}\overline{S}_{k-j}/abc$	0.21146	0.18756	0.13834	0.08953	0.06627	0.04372	0.02364	0.01234	0.008342	0.005059	0.002549	
0.10	A_kF_{k-j}/b^2		0.02819	0.03622	0.04086	0.04229	0.04325	0.04376	0.04390	0.04393	0.04394	0.04394	0.04395
	$A_kF_{k-j}\overline{S}_{k-j}/abc$		0.20379	0.17742	0.12737	0.09795	0.06659	0.03676	0.01944	0.013184	0.008018	0.004049	
0.20	A_kF_{k-j}/b^2			0.05421	0.06859	0.07377	0.07744	0.07942	0.07999	0.08010	0.08015	0.08018	0.08018
	$A_kF_{k-j}\overline{S}_{k-j}/abc$			0.18854	0.15900	0.13028	0.09337	0.05356	0.02890	0.01972	0.012047	0.006103	
0.40	A_kF_{k-j}/b^2				0.10013	0.11524	0.12770	0.13514	0.13736	0.13779	0.13801	0.13811	0.13814
	$A_kF_{k-j}\overline{S}_{k-j}/abc$				0.16255	0.14686	0.11517	0.07088	0.03903	0.02666	0.01697	0.008642	
0.60	A_kF_{k-j}/b^2					0.13888	0.16138	0.17657	0.18143	0.18239	0.18289	0.18311	0.18318
	$A_kF_{k-j}\overline{S}_{k-j}/abc$					0.14164	0.11940	0.07830	0.04467	0.03109	0.02025	0.010366	
1.0	A_kF_{k-j}/b^2						0.20004	0.23285	0.24522	0.24783	0.24921	0.24980	0.25000
	$A_kF_{k-j}\overline{S}_{k-j}/abc$						0.11121	0.08137	0.04935	0.03502	0.02196	0.01175	

2.0	$A_k F_{k-j}/b^2$	0.29860	0.33462	0.34386	0.34916	0.35142	0.35222
	$A_k F_{k-j} \bar{S}_{k-j} / abc$	0.07086	0.04924	0.03670	0.02401	0.01325	
4.0	$A_k F_{k-j}/b^2$		0.40544	0.43104	0.44840	0.45708	0.46020
	$A_k F_{k-j} \bar{S}_{k-j} / abc$		0.04051	0.03284	0.02320	0.01300	
6.0	$A_k F_{k-j}/b^2$			0.46932	0.49986	0.51744	0.52368
	$A_k F_{k-j} \bar{S}_{k-j} / abc$			0.02832	0.02132	0.01272	
10.0	$A_k F_{k-j}/b^2$				0.5502	0.5876	0.6053
	$A_k F_{k-j} \bar{S}_{k-j} / abc$				0.01759	0.01146	
20.0	$A_k F_{k-j}/b^2$					0.6608	0.7156
	$A_k F_{k-j} \bar{S}_{k-j} / abc$					0.008975	

TABLE B.3 Approximate band limits for parallel-plate geometry [Edwards and Nelson (1962), Edwards (1962), Edwards et al. (1967)]

Gas	Band center λ, μm	Band center η, cm^{-1}	Band limits η, cm^{-1}[a] Lower	Upper
CO_2	15	667	$667 - (\bar{A}_{15}/1.78)$	$667 + (\bar{A}_{15}/1.78)$
	10.4	960	849	1013
	9.4	1060	1013	1141
	4.3	2350	$2350 - (\bar{A}_{4.3}/1.78)$	2430
	2.7	3715	$3715 - (\bar{A}_{2.7}/1.76)$	3750
H_2O	6.3	1600	$1600 - (\bar{A}_{6.3}/1.6)$	$1600 + (\bar{A}_{6.3}/1.6)$
	2.7	3750	$3750 - (\bar{A}_{2.7}/1.4)$	$3750 + (\bar{A}_{2.7}/1.4)$
	1.87	5350	4620	6200
	1.38	7250	6200	8100

[a] $\bar{A}$ is found for various bands as in Example A.1. Terms such as $\bar{A}_{15}/1.78$ are $\bar{A}/2\left(1-\tau_g\right)$ from Equation 17 and Tables 1 and 2 of Edwards and Nelson (1962).

EXAMPLE B.2 Two black parallel plates are D = 1 m apart. The plates are of width W = 1 m and have infinite length normal to the cross section shown. Between the plates is carbon dioxide gas at $p_{CO_2} = 1$ atm and T_g = 1000 K. If plate 1 is at 2000 K and plate 2 is at 500 K, find the energy flux that must be supplied to plate 2 to maintain its temperature. The surroundings are at $T_e << 500$ K.

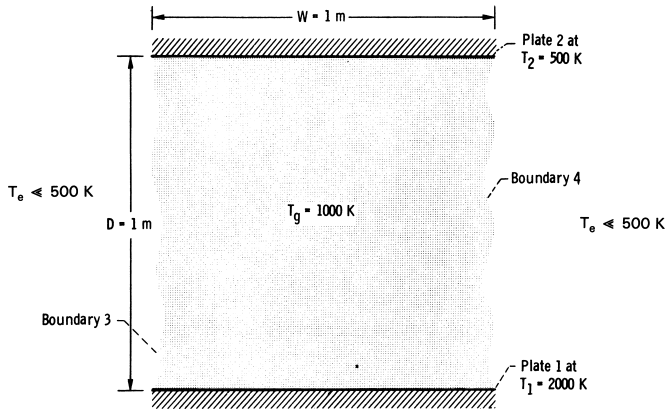

The geometry is a four-boundary enclosure formed by two plates and two open planes. The open areas are perfectly absorbing (nonreflecting) and radiate no significant energy as the surrounding temperature is low. The energy flux added to surface 2 is found by using the enclosure Equation 10.74 of the text where k = 2 and N = 4. All surfaces are black, $\epsilon_{\lambda,j}$ = 1, so Equation 10.74 reduces to

$$\sum_{j=1}^{4} \delta_{2j} q_{\lambda,j} = \sum_{j=1}^{4} [(\delta_{2j} - F_{2-j}\overline{\tau}_{\lambda,2-j}) e_{\lambda b,j} - F_{2-j}\overline{\alpha}_{\lambda,2-j} e_{\lambda b,g}] \tag{B.18}$$

The self-view factor F_{2-2} = 0 and $E_{\lambda b,3} = E_{\lambda b,4} \approx 0$, so this becomes

$$q_{\lambda,2} = -F_{2-1}\overline{t}_{\lambda,2-1} E_{\lambda b,1} + E_{\lambda b,2} - (F_{2-1}\overline{\alpha}_{\lambda,2-1} + F_{2-3}\overline{\alpha}_{\lambda,2-3} + F_{2-4}\overline{\alpha}_{\lambda,2-4}) E_{\lambda b,g} \tag{B.19}$$

To simplify the example, it is carried out by considering the entire wavelength region as a single spectral band. To obtain the total energy supplied to plate 2, integrate over all wavelengths to obtain

$$q_2 = -F_{2-1}\int_0^\infty \overline{t}_{\lambda,2-1} E_{\lambda b,1} d\lambda + \sigma T_2^4 - \int_0^\infty (F_{2-1}\overline{\alpha}_{\lambda,2-1} + F_{2-3}\overline{\alpha}_{\lambda,2-3} + F_{2-4}\overline{\alpha}_{\lambda,2-4}) E_{\lambda b,g} d\lambda$$

By use of the definitions of total transmission and absorption factors,

$$\overline{t}_{2-1}\sigma T_1^4 = \int_0^\infty \overline{t}_{\lambda,2-1} E_{\lambda b,1} d\lambda \qquad \overline{\alpha}_{2-1}\sigma T_g^4 = \int_0^\infty \overline{\alpha}_{\lambda,2-1} E_{\lambda b,g} d\lambda$$

and so forth, q_2 becomes

$$q_2 = \sigma T_2^4 - F_{2-1}\bar{t}_{2-1}\sigma T_1^4 - (F_{2-1}\bar{\alpha}_{2-1} + F_{2-3}\bar{\alpha}_{2-3} + F_{2-4}\bar{\alpha}_{2-4})\sigma T_g^4 \tag{B.20}$$

To determine $\bar{t}$ and $\bar{\alpha}$, the geometric-mean beam length is used. For opposing rectangles (Figure B.8 of this Appendix) at an abscissa of 1.0 and on the curve for a length-to-spacing ratio of ∞, the $\bar{S}_{2-1}/D = 1.34$, so $\bar{S}_{2-1} = 1.34$ m. To determine $\bar{\alpha}_{2-1}$, which determines the emission of the gas, use the emittance chart in Figure 9.18 or Equation 9.58 of the text at a pressure of 1 atm, L_e = 1.34 m and T_g = 1000 K. This gives $\bar{\alpha}_{2-1} = 0.22$. When obtaining $\bar{\tau}_{2-1}$, note from Equation B.20 that the radiation in the $\bar{\tau}_{2-1}$ term is $E_{\lambda b,1}$ and is coming from wall 1. Therefore it has a spectral distribution different from that of the gas radiation. To account for this nongray effect, Equation 10.121 is used with ϵ^+ evaluated at $p_{CO_2}\bar{S}_{2-1}(T_1/T_g) = 1.34(2000/1000) = 2.68$ atm · m and T_1 = 2000 K. Then, using Figure 9.18 (extrapolated) and Equation 10.121 of the text results in $\bar{\tau}_{2-1} \approx 1 - 0.2(\frac{1}{2})^{0.5} = 0.86$.

From Factor 3 in Appendix C of the text, the F_{2-1} is given by $F_{2-1} = [(D^2 + W^2)^{1/2} - D]/W = \sqrt{2} - 1 = 0.414$. Then $F_{2-3} = F_{2-4} = \frac{1}{2}(1 - 0.414) = 0.293$. The $\bar{\alpha}_{2-3} = \bar{\alpha}_{2-4}$, and they remain to be found. For adjoint planes, as in the geometry for Table B.2, the following expression from Equation 12 of Dunkle (1964) can be used, obtained for the present case where $b \to \infty$, a = 1, and c = 1: $\bar{S}_{2-3} = 2\ln\sqrt{2}/(\pi F_{2-3}) = 2 \times 0.347/(\pi \times 0.293) = 0.753$ m. Using Figure 9.18 $p\bar{S} = 0.753$ atm · m and T_g= 1000 K gives $\bar{\alpha}_{2-3} = \bar{\alpha}_{2-4} = 0.19$. Then the desired result is

$$\begin{aligned} q_2 &= \sigma T_2^4 - 0.414(0.86)\sigma T_1^4 - (0.414 \times 0.22 + 2 \times 0.293 \times 0.19)\sigma T_g^4 \\ &= 5.6704 \times 10^{-12}(500^4 - 0.36 \times 2000^4 - 0.20 \times 1000^4) \\ &= -33.4 \text{ W/cm}^2 \end{aligned}$$

Note that the largest contribution to q_2 is by energy leaving surface 1 that reaches and is absorbed by surface 2. Emission from the gas to surface 2, and emission from surface 2, are small.

An alternative approach for this particular example is to note that the term involving T_g in Equation B.20 is the flux received by surface 2 as a result of emission by the entire gas. This can be calculated from Equation 10.118 using the mean beam length. Then $q_2 = \sigma T_2^4 - F_{2-1}\bar{\tau}_{2-1}\sigma T_1^4 - \epsilon_g \sigma T_g^4$. For this symmetric geometry the average flux from the gas to one side of the enclosure is the same as that to the entire enclosure boundary. Consequently, the mean beam length can be obtained from Equation 10.114 as $L_e = 0.9(4)V/A = 0.9(4)(1 \text{ m})^2/4 \text{ m} = 0.9$ m. Then, from Figure 9.18 at T_g = 1000 K and $p_{CO_2}L_e = 0.9$ atm · m, the ϵ_g = 0.20. This gives the same q_2 as previously calculated.

HOMEWORK (Solutions are included in the Solution Manual under Chapter 10)

B.1 Two opposed parallel rectangles are separated by a distance of 0.5 m. The rectangles are of size 1.2 x 1.8 m. The space between the rectangles is filled with H_2O vapor at P = 1 atm and T = 1200 K. Assume for this calculation that only the 2.7-μm spectral band of H_2O participates in radiative absorption and emission by the gas, and use the data of Table A.2 of on-line Appendix A to compute ϵ_g. Rectangle 1 has T_1 = 1460 K, ϵ_1 = 1.0. Rectangle 2 has T_2 = 515 K, ϵ_2 = 0.6. Assume that the surroundings are at low temperature. Compute the total energy being added to each plate, using the method of Section 10.6.4 of the text.

B.2 A rectangular enclosure that is very long normal to the cross section shown has diffuse-gray walls at conditions shown below and encloses a uniform gray gas at T_g = 1500 K. The gas has an absorption coefficient of 0.25 m^{-1}. Find the average net radiative flux at each surface, and the energy necessary to maintain the gas at 1500 K.

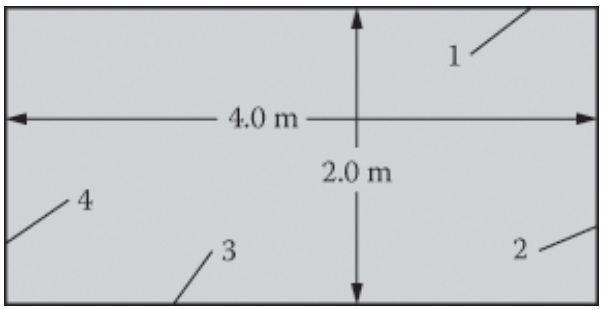

Surface	ϵ	T_w(K)
1	1.0	2000
2	0.5	1500
3	0.1	1000
4	0	500

Answer: q_1 = 607 kW/m^2; q_2 = − 75.1 kW/m^2; q_3 = − 39.3 kW/m^2;
energy added = 2,121 kW/m.

REFERENCES

Anderson, K. M., and Hadvig, S.: Geometric Mean Beam Lengths for a Space between Two Coaxial Cylinders, *JHT*, vol. 111, no. 3, pp. 811–813, 1989.

Dunkle, R. V.: Geometric Mean Beam Lengths for Radiant Heat-Transfer Calculations, *JHT*, vol. 86, no. 1, pp. 75–80, 1964.

Edwards, D. K.: Radiant Interchange in a Nongray Enclosure Containing an Isothermal Carbon Dioxide–Nitrogen Gas Mixture, *JHT*, vol. 84, no. 1, pp. 1–11, 1962.

Edwards, D. K., and Nelson, K. E.: Rapid Calculation of Radiant Energy Transfer between Nongray Walls and Isothermal H_2O or CO_2 Gas, *JHT*, vol. 84, no. 4, pp. 273–278, 1962.

Edwards, D. K., Glassen, L. K., Hauser, W. C., and Tuchscher, J. S.: Radiation Heat Transfer in Nonisothermal Nongray Gases, *JHT*, vol. 89, no. 3, pp. 219–229, 1967.

Hottel, H. C, and Sarofim, A. F.: *Radiative Transfer*, McGraw–Hill, New York, 1967.

Appendix C: Exponential Kernel Approximation

The solution for a gray medium in radiative equilibrium without internal heat sources between diffuse-gray walls was derived in Section 11.4.5 of the text in terms of the functions ψ_b and ϕ_b, that have been evaluated numerically and are in Table 11.2 and Figure 11.4 of the text. An approximate solution for ψ_b and ϕ_b is found here by using an approximation for the exponential integrals in the radiative flux equation. The ψ_b and ϕ_b are for black walls, so that $J_1 = \sigma T_{w1}^4$ and $J_2 = \sigma T_{w2}^4$ Without convection, conduction, or internal heat sources, the radiative flux q_r is independent of position and is equal to the flux q transferred between the walls. Then, with the dimensionless forms in Equation 11.55 of the text, Equation 11.49 relating the flux and temperature distribution becomes

$$\psi_b = 2E_3(\tau) + 2\int_{\tau^*=0}^{\tau} \phi_b(\tau^*) E_2(\tau - \tau^*) d\tau^* - 2\int_{\tau^*=\tau}^{\tau_D} \phi_b(\tau^*) E_2(\tau^* - \tau) d\tau^* \qquad \text{(C.1)}$$

From Appendix D of the text, the E_2 and E_3 are closely approximated by the exponential functions $E_2(\tau) \cong \frac{3}{4}\exp\left(-\frac{3}{2}\tau\right)$ $E_3(\tau) \cong \frac{1}{2}\exp\left(-\frac{3}{2}\tau\right)$. These approximations are inserted into Equation C.1 to yield

$$\psi_b = e^{-3\tau/2} + \frac{3}{2}e^{-3\tau/2}\int_{\tau^*=0}^{\tau} \phi_b(\tau^*) e^{-3\tau^*/2} d\kappa^* - \frac{3}{2}e^{3\tau/2}\int_{\tau^*=\tau}^{\tau_D} \phi_b(\tau^*) e^{-3\tau^*/2} d\tau * \qquad \text{(C.2)}$$

To solve for ψ_b and ϕ_b, Equation C.2 is differentiated twice with respect to τ, and, to satisfy the heat flux being constant across the distance between the walls, $d\psi_b/d\tau = 0$. This yields

$$0 = e^{-3\tau/2} + \frac{4}{3}\frac{d\phi_b}{d\tau} + \frac{3}{2}e^{-3\tau/2}\int_{\tau^*=0}^{\tau} \phi_b(\tau^*) e^{3\tau^*/2} d\tau^* - \frac{3}{2}e^{3\tau/2}\int_{\tau^*=\tau}^{\tau_D} \phi_b(\tau^*) e^{-3\tau^*/2} d\tau^* \qquad \text{(C.3)}$$

Equation C.3 is subtracted from Equation C.2 to give $\psi_b = -(4/3)(d\phi_b/d\tau)$. Since ψ_b, is a constant, this is integrated to yield

$$\phi_b = -\frac{3}{4}\psi_b \tau + C \qquad \text{(C.4)}$$

where C is an integration constant. The ψ_b, and C are found by substituting Equation C.4 back into the integral Equation C.2 to obtain

$$\psi_b = e^{-3\tau/2} + \frac{3}{2}e^{-3\tau/2}\int_{\tau^*=0}^{\tau}\left(-\frac{3}{4}\psi_b\tau^* + C\right)e^{3\tau^*/2} d\tau^* - \frac{3}{2}e^{3\tau/2}\int_{\tau^*=\tau}^{\tau_D}\left(-\frac{3}{4}\psi_b\tau^* + C\right)e^{-3\tau^*/2} d\tau^*$$

The integrations are carried out, and after simplification this becomes

$$0 = e^{-3\tau/2}\left(1 - \frac{1}{2}\psi_b - C\right) + e^{3(\tau-\tau_D)/2}\left(-\frac{3}{4}\psi_b\tau_D - \frac{1}{2}\psi_b + C\right)$$

Thus there are two simultaneous equations for ψ_b and C:

$$1-\frac{1}{2}\psi_b - C = 0 \text{ and } -\frac{3}{4}\psi_b\tau_D - \frac{1}{2}\psi_b + C = 0$$

The solution yields

$$\psi_b = \frac{1}{\frac{3}{4}\tau_D + 1} \tag{C.5a}$$

and $C = 1 - \psi_b/2$. These are substituted into Equation C.4 to give

$$\phi_b(\tau) = \frac{1}{\frac{3}{4}\tau_D + 1}\left[\frac{3}{4}(\tau_D - \tau) + \frac{1}{2}\right] \tag{C.5b}$$

Table C.1 compares Equation C.5*a* with the analytical results from Table 11.2 of the text; agreement is within about 3% for all τ_D.

TABLE C.1
Comparison of Dimensionless Radiative Flux in a One-Dimensional Slab by the Exponential Kernel Approximation with Exact Solution

	Dimensionless Radiative Flux, $\Psi_b(\tau_D)$	
τ_D	Equation C.5*a*	Text Table 11.2
0.2	0.8696	0.8491
0.4	0.7692	0.7458
0.6	0.6897	0.6672
1	0.5714	0.5532
1.5	0.4706	0.4572
2	0.4000	0.3900
3	0.3077	0.3016

The use of the approximate kernel for nongray media and for situations without radiative equilibrium is discussed in Gilles et al. (1969).

C. Exponential Kernel Approximation

REFERENCE:

Gilles, S. E., Cogley, A. C., and Vincenti, W. G.: A Substitute-Kernel Approximation for Radiative Transfer in a Non-Grey Gas near Equilibrium, with Application to Radiative Acoustics, *IJHMT*, vol. 12, pp. 445–458, 1969.

HOMEWORK

C.1 Consider a gray absorbing medium with isotropic scattering between parallel diffuse gray plates at temperatures T_1 and T_2, and spaced D apart. Heat conduction is negligible. Show that the exponential kernel approximation yields the same result for radiative heat transfer as obtained by the diffusion solution with jump boundary conditions. The medium has extinction coefficient β.

C.2 A gray gas is contained between infinite parallel plates. The plates both have emissivity $\epsilon = 0.30$. Plate 1 is held at temperature $T_1 = 1150$ K, and plate 2 is at $T_2 = 525$ K. The medium between the plates is nonscattering, and has a uniform absorption coefficient of $\kappa = 0.75$ m^{-1}. Heat conduction in the gas is neglected. The plane layer geometry is shown below.

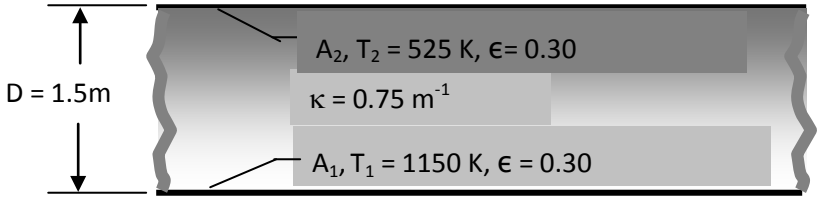

Predict the net radiative heat flux transferred between the surfaces (W/m^2) and plot the temperature profile $[T^4(\kappa) - T_2^4] / (T_1^4 - T_2^4)$ in the gas, where $\tau = \kappa x$. Solve the problem using the exponential kernel approximation. Compare the results with those of Homework Problems 12.6, 12.7 and 12.8.

(SOLUTIONS TO APPENDIX C PROBLEMS ARE IN THE SOLUTION MANUAL AT THE END OF CHAPTER 12 SOLUTIONS)

Appendix D: Curtis-Godson Approximation

For nonuniform gases a useful method for some radiation analyses is the Curtis-Godson approximation [Edwards and Weiner (1966), Krakow et al. (1966), Simmons (1966, 1968), Goody and Yung (1989)]. The transmittance of a given path through a nonisothermal gas is related to the transmittance through an equivalent isothermal gas. Then the solution is obtained by using isothermal-gas methods. The relation between the nonisothermal and the isothermal gas is found by assigning an equivalent amount of isothermal absorbing material to act in place of the nonisothermal gas. The amount is based on a scaling temperature and a mean density or pressure obtained in the analysis. These mean quantities are found by having the transmittance of the uniform gas be equal to the transmittance of the nonuniform gas in the weak and strong absorption limits.

Goody and Yung , Krakow et al., and Simmons discuss the Curtis-Godson method for attenuation in a narrow vibration-rotation band. Excellent comparisons with exact numerical results were obtained. Weiner and Edwards (1968) applied the method for steep temperature gradients in gases with overlapping band structures. Comparison of the analysis with experimental data was excellent. The Curtis-Godson technique is useful when the gas temperature distribution is specified. If the gas temperature distribution is not known, an iterative procedure would be needed; this is not very practical.

In this development, spectral variations are in terms of wave number, as is common for band correlations. For a nonuniform gas the absorption coefficient κ_η is variable along the path. An effective bandwidth $\bar{A}_l(S)$ is defined, analogous to Equation 9.23 of the text but using an integrated absorption coefficient:

$$\begin{aligned}\bar{A}_l(S) &= \int_{\substack{\text{absorption}\\ \text{bandwidth}}} \left\{1-\exp\left[-\int_0^S \kappa_\eta(S^*)dS^*\right]\right\} d\eta \\ &= \Delta\eta_l - \int_l \left\{\exp\left[-\int_0^S \kappa_\eta(S^*)dS^*\right]\right\} d\eta\end{aligned} \tag{D.1}$$

Similarly, for a path length from S^* to S, the effective bandwidth is

$$\bar{A}_l(S-S^*) = \int_{\substack{\text{absorption}\\ \text{bandwidth}}} \left\{1-\exp\left[-\int_{S^{**}=S^*}^S \kappa_\eta(S^{**})dS^{**}\right]\right\} d\eta \tag{D.2}$$

The integrated equation of transfer for intensity at S by radiation (without scattering) traveling from 0 to S is, from Equation 10.15 of the text,

$$\begin{aligned}I_\eta(S) &= I_\eta(0)\exp\left[-\int_{S^*=0}^S \kappa_\eta(S^*)dS^*\right] + \int_{S^*=0}^S \kappa_\eta(S^*)I_{\eta b}(S^*)\exp\left[-\int_{S^{**}=S^*}^S \kappa_\eta(S^{**})dS^{**}\right]dS^* \\ &= I_\eta(0)\exp\left[-\int_{S^*=0}^S \kappa_\eta(S^*)dS^*\right] - \int_{S^*=0}^S I_{\eta,b}(S^*)\frac{\partial}{\partial S*}\left\{1-\exp\left[-\int_{S^{**}=S^*}^S \kappa_\eta(S^{**})dS^{**}\right]\right\}dS^*\end{aligned} \tag{D.3}$$

Equation D. 3 is integrated over the bandwidth $\Delta\eta_l$, of the lth band, and the order of integration is changed on the last term. The $I_\eta(S)$, $I_\eta(\eta,0)$, and $I_{\eta b}(S)$ are approximated by average values within the band to yield

$$\begin{aligned} I_l(S)\Delta\eta_l &= I_l(0)\int_l \left\{\exp\left[-\int_{S^*=0}^{S}\kappa_\eta\left(S^*\right)dS^*\right]\right\}d\eta \\ &= -\int_{S^*=0}^{S} I_{l,b}\left(S^*\right)\frac{\partial}{\partial S^*}\int_l\left\{1-\exp\left[-\int_{S^{**}=S^*}^{S}\kappa_\eta\left(S^{**}\right)dS^{**}\right]\right\}d\eta dS^* \end{aligned} \tag{D.4}$$

Equations D.1 and D.2 are substituted into Equation D.4 to obtain the radiative transfer equation in terms of the $\bar{A}_l$.

$$I_l\left(S\right)\Delta\eta_l = I_l\left(0\right)\left[\Delta\eta_l - \bar{A}_l\left(S\right)\right] - \int_{S^*=0}^{S} I_{l,b}\left(S^*\right)\frac{\partial\bar{A}_l\left(S-S^*\right)}{\partial S^*}dS^* \tag{D.5}$$

An alternative form is found by integrating Equation D.5 by parts to obtain

$$I_l\left(S\right)\Delta\eta_l = I_l\left(0\right)\left[\Delta\eta_l - \bar{A}_l\left(S\right)\right] + I_{l,b}\left(0\right)\bar{A}_l\left(S\right) + \int_{S^*=0}^{S}\bar{A}_l\left(S-S^*\right)\frac{dI_{l,b}\left(S^*\right)}{dS^*}dS^* \tag{D.6}$$

Equations D.5 and D.6 are nearly exact forms of the integrated RTE in terms of the band properties. The only approximation is that the intensity in each term does not vary significantly across the wave number span of the band. For a uniform gas, Equation D.6 gives (since $dI_{l,b}/dS$ = 0)

$$I_{l,u}\left(S\right)\Delta\eta_l = I_l\left(0\right)\left[\Delta\eta_l - \bar{A}_{l,u}\left(S\right)\right] + I_{l,b,u}\left(0\right)\bar{A}_{l,u}\left(S\right) \tag{D.7}$$

where the u subscript denotes a uniform gas.

To compute $I_l(S)$ or $I_{l,u}(S)$ from Equations D.5, D.6, or D.7, expressions are needed for the effective bandwidth $\bar{A}_l$ for nonuniform and uniform gases. From Equations 9.16 and 9.20 of the text, the limiting cases of $\bar{A}_l$ for bands of independent weak or Lorentz strong absorption lines in a uniform gas have the forms

$$\bar{A}_{l,u}(S) = C_{1,l}\rho S_u \tag{D.8a}$$

$$\bar{A}_{l,u}(S) = C_{2,l}\rho_u S_u^{1/2} \tag{D.8b}$$

where $C_{l,,1}$ and $C_{2,l}$ are coefficients of proportionality for the lth band, and S_c and γ_c for the lines have been taken as proportional to gas density. For the nonuniform gas the effective bandwidth depends on the variation of properties along the path. The effective bandwidths are obtained by using Equations D.8a and D.8b locally along the path. This gives, for a band of weak lines,

$$\bar{A}_l(S) = C_{1,l}\int_{S^*=0}^{S}\rho(S^*)\,dS^* \qquad \text{(weak)} \tag{D.9a}$$

Similarly, for a band of strong lines, after first squaring Equation D.8b, $\bar{A}_l^2(S) = C_{2,l}^2 \int_{S^*=0}^{S} \rho^2(S^*)\, dS^*$, so that

$$\bar{A}_l(S) = C_{2,l}\left[\int_0^S \rho^2(S^*)\, dS^*\right]^{1/2} \qquad \text{(strong)} \tag{D.9b}$$

It is assumed that the $C_{1,l}$ and $C_{2,l}$ do not vary along the path.

In the Curtis-Godson method the nonuniform gas is replaced by an effective amount of uniform gas such that the correct intensity is obtained at the weak and strong absorption limits. To have the uniform intensity equal the nonuniform intensity, equate Equations D.7 and D.6 and simplify to obtain

$$\left[I_{l,b,u}(T_u) - I_l(0)\right]\bar{A}_{l,u}(S) = \left[I_{l,b}(0) - I_l(0)\right]\bar{A}_l(S) + \int_{S^*=0}^{S} \bar{A}_l(S - S^*)\frac{dI_{l,b}(S^*)}{dS^*}\, dS^* \tag{D.10}$$

To have Equation D.10 valid at the weak absorption limit, substitute $\bar{A}_{l,u}$ from Equation D.8a and $\bar{A}_l$ from Equation D.9a to obtain the following after canceling the $C_{1,l}$.

$$\begin{aligned}&\left[I_{l,b,u}(T_u) - I_l(0)\right]\rho_u S_u \\ &\quad = \left[I_{l,b}(0) - I_l(0)\right]\int_{S^*=0}^{S} \rho(S^*)dS^* + \int_{S^*=0}^{S}\left[\int_{S^{**}=S^*}^{S} \rho(S^{**})dS^{**}\right]\frac{dI_{l,b}(S^*)}{dS^*}\, dS^*\end{aligned} \tag{D.11a}$$

Similarly, at the strong absorption limit, insert Equations D.8b and D.9b into Equation D.10 to obtain

$$\begin{aligned}\left[I_{l,b,u}(T_u) - I_l(0)\right]\rho_u S_u^{1/2} &= \left[I_{l,b}(0) - I_l(0)\right]\left[\int_{S^*=0}^{S} \rho^2(S^*)dS^*\right]^{1/2} \\ &\quad + \int_{S^*=0}^{S}\left[\int_{S^{**}=S^*}^{S} \rho^2(S^{**})dS^{**}\right]^{1/2}\frac{dI_{l,b}(S^*)}{dS^*}\, dS^*\end{aligned} \tag{D.11b}$$

For known temperature and density distributions in a nonuniform gas, Equations D.11a. and D.11b are solved simultaneously for ρ_u and S_u, which are the equivalent uniform gas density and path length for that particular band. The $I_{l,b,u}(T_u)$ is not an additional unknown since the temperature T_u corresponds to ρ_u through the ideal gas law. Then Equation D.7 can be used for any effective bandwidth dependence on ρ_u and S_u (that is, not only at the weak and strong limits) to solve for $I_{l,u}(S)$. This exactly equals $I_l(S)$ in the nonuniform gas in the weak and strong limits and is usually a good approximation for intermediate absorption values. Once the intensities are found, the radiative transfer is obtained by using the relations for a uniform gas. Evaluating Equations D.11a. and D.11b usually requires numerical integration. Because the Curtis-Godson method requires evaluating at least two integrals for each band along each path, it may be equally feasible to numerically evaluate the nearly exact forms Equation D.5 or D.6.

D: Curtis-Godson Approximation

As originally formulated [Goody and Yung (1989)], the Curtis-Godson method was limited to a small wave number span in an absorption band. The limitation was because of line overlapping and the change in the number of important lines with temperature. It has been shown in Weiner and Edwards (1968) and Plass (1967) that the method gives good results even for conditions with large temperature gradients with the use of fairly wide wave number spans. These references also account for overlapping absorption bands. A band absorption formulation analogous to the Curtis-Godson approximation but involving three parameters was developed by Cess and Wang (1970). The additional parameter enabled the equivalent isothermal gas to give the correct behavior in the linear and square-root limits, and also in the logarithmic limit for very strong absorption. The further treatment of radiative transfer along strongly nonisothermal paths is in Vitkin et al. (2000). To try to overcome spectral complexity, a Planck-Rosseland gray model has been developed; it is applied to a hypersonic radiating flow in Sakai et al. (2001).

REFERENCES:

Cess, R. D., and Wang, L. S.: A Band Absorptance Formulation for Nonisothermal Gaseous Radiation, *IJHMT*, vol. 13, no. 3, pp. 547–555, 1970.

Edwards, D. K., and Weiner, M. M.: Comment on Radiative Transfer in Nonisothermal Gases, *Combust. Flame*, vol. 10, no. 2, pp. 202–203, 1966.

Goody, R. M., and Yung, Y. L.: *Atmospheric Radiation*, 2d ed., Oxford University Press, New York, 1989.

Krakow, B., Babrov, H. J., Maclay, G. J., and Shabott, A. L.: Use of the Curtis-Godson Approximation in Calculations of Radiant Heating by Inhomogeneous Hot Gases, *Appl. Opt*., vol. 5, no. 11, pp. 1791–1800, 1966.

Plass, G. N.: Radiation from Nonisothermal Gases, *Appl. Opt*., vol. 6, no. 11, pp. 1995–1999, 1967.

Sakai, T., Tsuru, T., and Sawada, K.: Computation of Hypersonic Radiating Flow-Field over a Blunt Body, *JTHT*, vol. 15, no. 1, pp. 91–105, 2001.

Simmons, F. S.: Band Models for Non-isothermal Radiating Gases, *Appl. Opt*., vol. 5, no. 11, pp. 1801–1811, 1966.

Simmons, F. S.: Application of Band Models to Inhomogeneous Gases, Molecular Radiation and Its Application to Diagnostic Techniques (R. Goulard, ed.), NASA TM X-53711, pp. 113–133, 1968.

Vitkin, E. I., Shuralyov, S. L., and Tamanovich, V. V.: Engineering Procedure for Calculating the Transfer of the Selective Radiation of Molecular Gases, *IJHMT*, vol. 43, no. 11, pp. 2029–2045, 2000.

Weiner, M. M., and Edwards, D. K.: Nonisothermal Gas Radiation in Superposed Vibration-Rotation Bands, *JQSRT*, vol. 8, no. 5, pp. 1171–1183, 1968.

E. RADIATIVE TRANSFER IN POROUS AND DISPERSED MEDIA

Radiative transfer in porous and dispersed media is reviewed in Tien (1988), Dombrovsky (1996), Baillis-Doermann and Scadura (1998), Howell (2000), Kamiuto (1999, 2008), Nakouzi (2012), and Schoegl (2012) which provide extensive bibliographies. Many early models neglected the effect of anisotropic and/or dependent scattering that have been found important in some applications. If the porous structure is well defined, newer models have moved toward numerical and statistical modeling approaches that incorporate the detailed porous structure and its thermal properties. Considering radiative transfer among the structural elements provides detailed radiative transfer results, but does not yield simplified engineering heat transfer correlations. If the structural elements are translucent, refraction at the solid-fluid interfaces must be considered as well as the external and internal reflections that occur at these interfaces (see Section 17.5.3). Almost always, the structural elements are so closely spaced that dependent scattering occurs (Section 16.4). Independent scattering has been shown to fail for systems with low porosity and for packed beds [Singh and Kaviany (1994)], and deviations from independent scattering theory have been found at porosities as high as 0.935.

A less detailed engineering approach has been to assume that the porous material can be treated as a continuum. This depends on the minimum porous bed or medium dimension, L, relative to the particle or pore diameter, D_p or D_{pore}, and the particle size parameter $\xi = \pi D_P/\lambda$. For most practical systems the porous material is many pore or particle diameters in extent (L/D_{pore} or $L/D_p > \sim 10$), and the pores or particles are large relative to the wavelengths of the important radiative energy ($\xi > \sim 5$). In this case, the porous medium may be treated as continuous, and the effective radiative properties are measured by averaging over the pore structure. Traditional radiative transfer analysis methods for translucent media can then be applied without using detailed element-to-element modeling. When temperature gradients are large and/or the thermal conductivity of the elements is small, the assumption of isothermal elements may not be accurate [Singh and Kaviany (1994)]. Combustion in some liquid- and gas-fueled porous burners occurs within the porous structure, producing large temperature gradients; temperatures within the porous medium can increase by over 1000 K within a few pore diameters.

The energy equation for porous media analysis depends on the complexity of the particular problem to be solved. To determine the energy transfer between the porous solid and a flowing fluid, energy equations are written for both the solid and the fluid, with a convective transfer term providing the coupling between the two equations. This approach permits calculation of the differing bed and fluid temperatures. If the fluid is transparent (no absorption or scattering) the radiative flux divergence is only in the equation for the absorbing and radiating solid structure of the porous material. In this case, the energy equations (in one dimension) become, for the fluid and solid phases,

$$\rho u c_p \frac{dT_f}{dx} - \frac{d}{dx}\left(k_f \frac{dT_f}{dx} \right) - \dot{q} + h_v (T_f - T_s) = 0 \tag{E.1}$$

$$\frac{d}{dx}\left(k_s \frac{dT_s}{dx} \right) - \frac{dq_r}{dx} + h_v (T_f - T_s) = 0 \tag{E.2}$$

The h_v is the volumetric convective heat transfer coefficient, and $\dot{q}$ is the volumetric energy source in the fluid from combustion or other internal energy sources. The properties are effective properties that depend on the structure of the solid and the flow configuration. If multiple species are present, as for combustion, additional terms for species diffusion must be included in the fluid-phase equation. The coupling of Equations E.1 and E.2 through the convective transfer terms shows that radiation affects both the solid and fluid temperature distributions even when a radiation term is only in the solid energy equation.

If there is no fluid within the porous medium, a single energy equation is used for the temperature distribution of the solid structure. Then Equations E.1 and E.2 reduce to the steady form of Equation 10.3 of the text with no viscous dissipation. Alternatively, if the fluid flow rate is sufficiently large, the volumetric heat transfer coefficient becomes large and the local fluid and solid temperatures become essentially equal; then Equations E.1 and E.2 combine to give

$$\rho u c_p \frac{dT}{dx} - \frac{d}{dx}\left(k_{\text{eff}} \frac{dT}{dx} \right) + \frac{dq_r}{dx} - \dot{q} = 0 \qquad \text{(E.3)}$$

In this equation, k_{eff} is the effective thermal conductivity of the fluid-saturated porous medium, and the other properties are corrected for the porosity and are on a per unit of total volume basis.

Most analyses of radiative transfer in porous media rely on solving the radiative transfer equation (RTE) and it is necessary to measure or predict the effective continuum radiative properties of the porous medium. This can be done by direct or indirect measurements, or by predicting the properties using models of the geometrical structure and surface properties of the porous structural material. Most radiative property measurements are made by inferring the detailed properties from measurement of radiative transmission or reflection by the porous material. Measured and predicted properties of various packed beds are discussed in Howell (2000), and the properties of open-cell foam insulation are studied in Baillis et al. (2000). Haussener et al. (2009) use computerized tomography to determine the physical characteristics of a packed bed of $CaCO_3$ particles, and then use forward Monte Carlo to determine the spectral scattering and absorption coefficients as well as the spectral phase function. Although the results were independent of the reflectivity characteristics of the system boundaries (specular or diffuse), they were strongly dependent on the assumed reflectivity characteristics of the particles.

Solutions are difficult when the radiative mean free path is of the order of the overall bed dimensions. Simplifying assumptions cannot be made, such as an optically thick medium, and in this case a complete solution of the RTE may be required. The two-flux method is often used when one-dimensional radiative transfer is assumed; however, if the particles in the bed are absorbing, this method does not give satisfactory results [Singh and Kaviany (1994)]. If the solid structure of the porous medium has a defined shape it is possible to use conventional surface-to-surface radiative interchange analysis. This is used in Antoniak et al. (1996) and Palmer et al. (1996) with a Monte Carlo cell-by-cell analysis to simulate radiative transfer among arrays of geometric shapes. Some research has tried to define an effective radiative conductivity that can be combined with heat conduction. For use in optically thick systems with porosity between 0.4 and 0.5, composed of opaque solid spherical particles with surface emissivity ϵ_r and thermal

conductivity of the solid k_s, the radiative conductivity can be approximated by [Singh and Kaviany (1991, 1994), Kaviany (1991)]:

$$k_r = 4D_p\sigma T^3\left\{0.5756\epsilon_r \tan^{-1}\left[1.5353(k_s^*)^{0.8011}/\epsilon_r\right]+0.1843\right\} \qquad \text{(E.4)}$$

where $k_s^* = k_s/(4D_p\sigma T^3)$. This is reasonably accurate for both diffuse and specular reflecting particles [the constants in (E.4) from are specifically for diffuse surfaces], and is weakly dependent on bed porosity.

An early work on radiation transfer in dispersed media was by Viskanta and Mengüç (1989). Baillis and Sacadura (1996, 2000) have expanded the concept and provided a through literature search. Transport phenomena, including radiation models in solid gas foams were given by Pilon et al. (2001) and for glass foams the state-of-the-art was discussed by Federov and Pilon (2002). Further applications to foams were reported in a number of studies by Baillis's group [Loretz et al. (2008);); Randrianalisoa et al. 2006; Randrianalisoa and Baillis (2010, 2014); Kaemmerlen et al. (2010); Coquard et al. (2012)]. Diagnosis of foamy and bubbly media also require understanding of radiative transfer and light scattering concepts, as discussed by Wong and Mengüç (2002); Vaillon et al. (2004); Aslan et al. (2006); Swamy et al. (2007); and Gay et al. (2010). A recent monograph on dispersed systems has summarized many formulations and applications specific to practical problems [Dombrovsky and Baillis (2010)]. The case of long cylindrical fibers in random orientations is analyzed for the geometric optics region using a detailed Monte Carlo analysis in Nisipeanu and Jones (2003). Particle suspensions in liquid are studied in Ma et al. (2015).

REFERENCES:

Antoniak, Z. L., Palmer, B. J., Drost, M. K., and Welty, J. R.: Parametric Study of Radiative Heat Transfer in Arrays of Fixed Discrete Surfaces, *JHT*, vol. 118, no. 1, pp. 228–230, 1996.

Aslan, M. M., Crofcheck, C., Tao, D., and Mengüç, M. P.: Evaluation of Micro Bubble Size and Gas Holdup in Two Phase Gas-Liquid Columns via Scattered Light Measurements, *JQSRT*, vol. 101, pp. 527–539, 2006.

Baillis, D., and Sacadura, J.F.: Heat Transfer in Open Cell Foam Insulations, *JHT*, vol. 118, no. 1, pp. 292-298, 1996.

Baillis-Doermann, D., and Sacadura, J. F.: Thermal Radiation Properties of Dispersed Media: Theoretical Prediction and Experimental Characterization, *JQSRT*, vol. 67, no. 5, pp. 327-363, 2000.

Baillis, D., Raynaud, M., and Sacadura, J. F.: Determination of Spectral Radiative Properties of Open-Cell Foam: Model Validation, *JTHT*, vol. 14, no. 2, pp. 137–143, 2000.

Coquard, R., Rochais, D., and Baillis, D.: Conductive and Radiative Heat Transfer in Ceramic and Metal Foams at Fire Temperatures, *Fire Tech.*, vol. 48 no. 3, pp. 699-732, 2012.

Dombrovsky, L. A.: *Radiation Heat Transfer in Disperse Systems*, Begell House, New York, 1996.

Dombrovsky, L.A., and Baillis, D.: Thermal Radiation in Disperse Systems: An Engineering Approach, Begell House, 2010.

Fedorov, A.G., and Pilon, L.: Glass Foams: Formation, Transport Properties, and Heat, Mass, and Radiation Transfer, *J. Non-Crystalline Solids*, vol. 311, no. 2, pp. 154-173, 2002.

Gay, B., Vaillon R., and Menguc, M. P.: Polarization Imaging of Multiply-scattered Radiation Based on Integral-Vector Monte Carlo Method, *JQSRT*, vol. 111, pp. 287-294, 2010.

Haussener, S., Lipiński, W., Petrasch, J., Wyss, P., and Steinfeld, A.: Tomographic Characterization of a

Semitransparent-Particle Packed Bed and Determination of Its Thermal Radiative Properties, *JHT*, vol. 131, no. 7, pp. 072701–072712, July, 2009.

Howell, J. R.: Radiative Transfer in Porous Media, in K. Vafai (ed.), *Handbook of Porous Media*, Chap. 7, Marcel Dekker, New York, 2000.

Kaemmerlen, A., Vo, C., Asllanaj, F., Jeandel, G., and Baillis, D.: Radiative Properties of Extruded Polystyrene Foams: Predictive Model and Experimental Results, *JQSRT*, vol. 111. no. 6, pp. 865-877, 2010.

Kamiuto, K.: Modeling of Elementary Transport Processes and Composite Heat Transfer in Open-Cellular Porous Materials, in *Trends in Heat, Mass and Momentum Transfer*, U. Ramchandran, exec. ed., vol. 5, pp. 141–161, *Research Trends*, Trivandrum, India, 1999.

Kamiuto, K.: Modeling of Composite Heat Transfer in Open-Cellular Porous Materials at High Temperatures, in A. Achsner, G. E. Murch, and M. J. S. de Lemos (eds.), *Cellular and Porous Materials: Thermal Properties Simulation and Prediction*, Wiley-VCH, Weinheim, 2008.

Kaviany, M.: *Principles of Heat Transfer in Porous Media*, Springer-Verlag, New York, 1991.

Loretz, M., Coquard, R., Baillis, D., and Maire, E.: Metallic Foams Radiative Properties/Comparison between Different Models, *JQSRT*, vol. 109, no. 1, pp. 16-27, 2008.

Ma, C.Y., Zhao, J.M., Liu, L.H., and Zhang, L.: GPU-Accelerated Inverse Identification of Radiative Properties of Particle Suspensions in Liquid by Monte Carlo, *Proc. 5th Int. Symp. Computational Thermal Radiation in Participating Media*, Albi, France, 1-3 April, 2015.

Nakouzi, S.: *Modelization du Procédé de Cuisson de Composites Infusés par Chauffage Infra Rouge*, doctoral thesis, Institut Clément Ader, Ecole des Mines d'Albi, l'Université de Toulouse, Albi, France, 2012.

Nisipeanu, E. and Jones, P.: Monte Carlo Simulation of Radiative Heat Transfer in Course Fibrous Media, *JHT*, vol. 125, pp. 748-752, 2003.

Palmer, B. J., Drost, M. K., and Welty, J. R.: Monte Carlo Simulation of Radiative Heat Transfer in Arrays of Fixed Discrete Surfaces Using Cell-to-Cell Photon Transport, *IJHMT*, vol. 39, no. 13, pp. 2811–2819, 1996.

Pilon, L., Fedorov, A.G., and Viskanta, R.: Steady-state Thickness of Liquid–gas Foams, *J. of Colloid and Interface Science*, vol. 242, no. 2, pp. 425-436, 2001.

Randrianalisoa, J., and Baillis, D.: Radiative Properties of Densely Packed Spheres in Semitransparent Media: A New Geometric Optics Approach, *JQSRT*, vol. 111, no. 10, pp. 1372-1388, 2010.

Randrianalisoa, J.H., and Baillis, D.: Analytical Model of Radiative Properties of Packed Beds and Dispersed media, *IJHMT*, vol. 70, pp. 264-275, 2014.

Randrianalisoa, J.H., Dombrovsky, L.A., Lipiński, W., and Timchenko, V.: Effects of Short-Pulsed Laser Radiation on Transient Heating of Superficial Human Tissues, *IJHMT*, vol. 78, pp. 488-497, 2014.

Schoegl, I.: Radiation Effects on Flame Stabilization on Flat Flame Burners, *Comb.and Flame*, vol. 159, no. 9, pp. 2817-2828, 2012.

Singh, B. P., and Kaviany, M.: Independent Theory versus Direct Simulation of Radiative Heat Transfer in Packed Beds, *IJHMT*, vol. 34, pp. 2869–2881, 1991.

Singh, B. P., and Kaviany, M.: Effect of Solid Conductivity on Radiative Heat Transfer in Packed Beds, *IJHMT*, vol. 37, no. 16, pp. 2579–2583, 1994.

Swamy, J.N., Crofcheck, C., and Mengüç, M.P.: A Monte Carlo Ray Tracing Study of the Polarized Light Propagation in Liquid Foams, JQSRT, vol. 101, pp. 527-539, 2007.

Tien, C. L.: Thermal Radiation in Packed and Fluidized Beds, *JHT*, vol. 110, pp. 1230–1242, 1988.

Vaillon, R., Wong, B.T., and Mengüç, M.P.: Polarized Radiative Transfer in a Particle-laden Semi-transparent Medium via a Vector Monte Carlo Method, *JQSRT*, vol. 84, pp. 383-394, 2004.

Viskanta, R., and Mengüç, M. P.: Radiative Transfer in Dispersed Media, *ASME Appl. Mechanics Rev.*, vol. 42, pp. 241–259, 1989.

Wong, B., and Mengüç, M. P.: Depolarization of Radiation by Foams, *JQSRT*, vol. 73, nos. 2–5, pp. 273–284, 2002.

F. Benchmark Solutions for Verification of Radiation Solutions

TABLE F.1 Incident radiation $4\pi\bar{I}$ and z-component of radiative flux q_z in cube of side length $2c$ exposed to uniform diffuse incident radiation q_i on bottom surface $z = -c$ with nonhomogeneous gray extinction coefficient $\beta = (0.05/c) + (0.45/c)\{[1-(x^2/c^2)][1-(y^2/c^2)][1-(z^2/c^2)]\}^2$, isotropic scattering, and scattering albedo ω. Results tabulated along line z, $x = y = 0$. Results by numerical quadrature using 17 quadrature points (QM17) [Wu et al. (1996)] (origin of coordinates is at cube center)

	$4\pi\bar{I}(z)/q_i(-c)$		$q_z(z)/q_i(-c)$	
$z/(2c)$	$\omega = 1.0$	$\omega = 0.5$	$\omega = 1.0$	$\omega = 0.5$
−0.49529	2.0674	2.0205	0.9466	0.9746
−0.47534	1.9955	1.9427	0.9410	0.9691
−0.44012	1.8730	1.8107	0.9246	0.9525
−0.39076	1.7066	1.6302	0.8883	0.9150
−0.32884	1.5055	1.4120	0.8251	0.8478
−0.25635	1.2837	1.1745	0.7359	0.7508
−0.17562	1.0588	0.9416	0.6311	0.6355
−0.08924	0.8487	0.7345	0.5259	0,5197
0.00000	0.6667	0.5657	0.4325	0.4180
0.08924	0.5196	0.4374	0.3566	0.3374
0.17562	0.4081	0.3451	0.2987	0.2778
0.25635	0.3280	0.2813	0.2560	0.2357
0.32884	0.2729	0.2384	0.2252	0.2066
0.39076	0.2365	0.2100	0.2033	0.1867
0.44012	0.2131	0.1917	0.1882	0.1733
0.47534	0.1989	0.1803	0.1785	0.1647
0.49529	0.1914	0.1744	0.1734	0.1602

TABLE F.2 Integrated intensity $4\pi\bar{I}$ and surface heat flux distributions q_z, in cylinder with diameter $2r_o$ = height z_o exposed to uniform collimated incident flux $q_i = 1$ on top surface $z = 0$ (positive z extends vertically downward) with nonabsorbing gray homogeneous isotropic scattering, scattering coefficient σ_s, and optical thickness $\tau_{zo} = \sigma_s z_o = 0.25$. Results tabulated along radius $0 < r < r_o$ at z_1 and z_2, and along axial position $0 < z < z_o$ at r_1 and r_2. Results by numerical quadrature using 17 quadrature points (QM17) [Hsu et al. (1999)]

τ_r/τ_{ro}	$4\pi\bar{I}(\tau_r,\tau_{z1})$	$4\pi\bar{I}(\tau_r,\tau_{z2})$	$q_z^-(\tau_r,0)$	$q_z^+(\tau_r,\tau_{zo})$	τ_z/τ_{zo}	$4\pi\bar{I}(\kappa_{r1},\kappa_z)$	$4\pi\bar{I}(\tau_{r2},\tau_z)$	$q_r^+(\tau_{ro},\tau_z)$
0.015625	1.08356	0.85828	0.04490	0.81969	0.015625	1.08356	1.04819	0.02810
0.078125	1.08344	0.85819	0.04484	0.81964	0.078125	1.09101	1.04359	0.03485
0.140625	1.08313	0.85790	0.04464	0.81944	0.140625	1.08377	1.03439	0.03913
0.203125	1.08260	0.85742	0.04434	0.81915	0.203125	1.07618	1.02194	0.04052
0.265625	1.08188	0.85678	0.04390	0.81873	0.265625	1.06548	1.00914	0.04168
0.328125	1.08096	0.85595	0.04337	0.81824	0.328125	1.05352	0.99588	0.04252
0.390625	1.07980	0.85490	0.04271	0.81761	0.390625	1.04008	0.98229	0.04302
0.453125	1.07844	0.85370	0.04194	0.81689	0.453125	1.02603	0.96805	0.04293
0.515625	1.07688	0.85233	0.04106	0.81609	0.515625	1.01082	0.95352	0.04252
0.578125	1.07509	0.85076	0.04006	0.81519	0.578125	0.99534	0.93892	0.04194
0.640625	1.07303	0.84899	0.03892	0.81417	0.640625	0.97851	0.92381	0.04088
0.703125	1.07059	0.84686	0.03749	0.81286	0.703125	0.96127	0.90835	0.03942
0.765625	1.06747	0.84405	0.03557	0.81106	0.765625	0.94304	0.89258	0.03771
0.828125	1.06363	0.84070	0.03334	0.80902	0.828125	0.92268	0.87656	0.03583
0.890625	1.05879	0.83654	0.03064	0.80660	0.890625	0.90140	0.85956	0.03307
0.984375	1.04819	0.82775	0.02527	0.80204	0.984375	0.85828	0.82775	0.02462

[a] $\tau_{r1} = \tau_{ro}/64$, $\tau_{r2} = 63\,\tau_{ro}/64$, $\tau_{z1} = \tau_{zo}/64$, $\tau_{z2} = 63\,\tau_{zo}/64$.

Table F.3 Listing of Benchmark Solution References: Absorbing/Emitting/scattering Media in Simple Enclosures

Geometry	Method	Parameter Range	Boundary Conditions	Comments	Reference
3-D, Cube	Finite element	Given spectral property variation, $\kappa(x,y,z)$; $\omega = 0, 0.9$	Cold, black walls, isothermal medium, isotropic scattering	Compares with YIX and MC solutions.	Burns et al. (1995)
2-D square enclosure	Analytical	All optical thickness	One hot wall, three cold walls; cold medium	Analytical solution; best reference for checking methods in 2-D	Crosbie and Shrenker (1982)
3-D, cube	Analytical	All optical thickness; all ω	One hot wall, 5 cold walls; cold medium, isotropic scattering	Analytical solution; best reference for checking methods in 3-D	Crosbie and Shrenker (1984)
3-D, cube	YIX	$\kappa(x,y,z)$; ω=0 or prescribed linear anisotropic	Cold, black walls, isothermal medium, no or anisotropic scattering	Discussion of error sources in YIX solution relative to exact analytical solution of Crosbie and Shrenker (1984)	Hsu and Tan (1996)
3-D, cube	Numerical quadrature	$\kappa(x,y,z)$; $\omega = 0.5, 1.0$	One hot wall, 5 cold walls; cold gray medium, isotropic scattering	Results in Table F.2	Hsu et al. (1999)
Cylinder with height = diameter	Numerical quadrature	$\tau = \sigma_s z_0 = 0.25$	Cold gray nonabsorbing medium, isotropic scattering, black cold walls except hot top.	Results in Table F.1	Wu et al. (1999)
3-D, cube	Discrete transfer and MC	Given spectral property variation, $\kappa(x,y,z)$; ω = 0, 0.5, 0.9	Cold, black walls, isothermal medium, linear anisotropic scattering	Examines error as a function of angular quadrature	Henson et al. (1997)
3-D, cube	YIX, MC	Given spectral property variation, $\kappa(x,y,z)$; ω = 0, 0.9	All cold, black walls, or 1 hot, 5 cold walls; isothermal medium, isotropic scattering		Hsu and Farmer (1997)
1-D, and 2-D, square	Product Integration	1-D; τ = 0.1, 0.5, 1.0, 3.0 and 3 anisotropic scattering values. 2-D: $\tau = 1$	3-D: 3 sdjacent cold black or diffuse gray walls; 1 hot wall, linear ansotropic scattering. Or, 4 cold black or diffuse gray walls, uniform internal generation, linear anisotropic scattering.	Proposes method to reduce order of integrations required for solution.	Tan (1998)

2-D square enclosure	M_1. S_{32}	$\tau = 5$	Black surfaces	Planar radiation sources at various locations within medium.	Gonzalez et al. (2008)
2-D square enclosure	S_4, S_6, M_1, P_1	$\tau = 0 – 10$, $\omega = 0$ - 1	One hot wall, three cold walls, all black	Compares accuracy of each method with analytical solution of Crosbie and Shrenker (1982)	Tencer and Howell (2013)
2-D square and 3-D cubical	S_8 and S_{16} for 2-D; S_4, S_8 and S_{12} for 3-D.	$\tau = 1$, pure scattering	Black surfaces; One hot wall, three cold walls ,isotropic scattering for 2-D; 1 hot, 5 cold walls, Henyey-Greenstein phase function for 3-D	General discussion of factors affecting accuracy of DOM with many references	Coelho (2014)
Annulus between concentric spheres	Analytical derivation with numerical evaluation of weighting functions	Any value of τ or β, $\omega = 0$ - 1 all radius ratios, all boundary temperatures.	Black or gray boundaries, gray medium, linear anisotropic scattering.	Compares results with prior solutions using various methods	Le Dez and Sadat (2015)

Some other benchmark solutions are in Spuckler and Siegel (1996), Olson et al. (2000), Tan et al. (2000), Gonzalez et al. (2009), Joseph et al. (2009)

REFERENCES

Burns, S. P., Howell, J. R., and Klein, D. E.: Finite Element Solution for Radiative Heat Transfer with Nongray, Nonhomogeneous Radiative Properties, *ASME HTD*-vol. 315, pp. 3–10, 1995.

Coelho, P.J.: Advances in the Discrete Ordinates and Finite Volume Methods for the Solution of Radiative Heat Transfer Problems in Participating Media, *JQSRT*, vol. 145, 241-246, 2014.

Crosbie, A. L., and Schrenker, R. G.: Radiative Transfer in a Two-Dimensional Rectangular Medium Exposed to Diffuse Radiation, *JQSRT*, vol. 31, no. 4, pp. 339-372, 1984.

Crosbie, A. L., and Schrenker, R. G.: Exact Expressions for Radiative Transfer in a Three-Dimensional Rectangular Geometry, *JQSRT,* vol. 28, pp. 507-526, 1982.

González, M., Velarde, P., and Garćıa-Fernández, C.: First Comparison of Two Radiative Transfer Methods: M1 and Sn Techniques, *ASP Conference Series*, Vol. 385, Nikolai V. Pogorelov, Edouard Audit, and Gary P. Zank, eds., 2008.

González, M., Garćıa-Fernández, C, and Velarde, P.: 2D Numerical Comparison between S_n and M_1 Radiation Transport Methods, *Annals of Nuclear Energy* , vol. 36, no. 7, pp. 886-895, 2009.

Henson, J. C, Malasekekera, W. M. G., and Dent, J. C.: Comparison of the Discrete Transfer and Monte Carlo Methods for Radiative Heat Transfer in Three-Dimensional, Nonhomogeneous Participating Media, *Num. Heat Transfer*, Part A, vol. 32, no. 1, pp. 19-36, July, 1997.

Hsu, P.-f., and Tan, Z.: Recent Benchmarkings of Radiative Heat Transfer within Nonhomogeneous Participating Media and the Improved YIX Method, Proc. Int. Symp. on Radiation Transfer, ed. by M.P. Mengüç, Kusadasi, Turkey, , pp.107-126, Begell House, Inc. NY, August 1995,

Hsu, P.-f, and Farmer, J. T.: Benchmark Solutions of Radiative Heat Transfer within Nonhomogeneous Participating Media Using the Monte Carlo and YIX Method, *JHT*, vol. 119, no. 1, pp. 185-188, 1997.

Hsu, P.-f., Tan, Z. -M., Wu, S. -H., and Wu, C. -Y.: Radiative Heat Transfer in the Finite Cylindrical Homogeneous and Nonhomogeneous Scattering Media Exposed to Collimated Radiation, *Numer. Heat Trans*, vol. 31, no. 8, pp. 819–836, 1999.

Le Dez, V., and Sadat, H.: Radiative Transfer in a Semitransparent Medium Enclosed in a Spherical Annulus, *Int. J. Thermal Sci.*, vol. X, no XX, 2015.

Joseph, D., Perez, P., El Hafi, M., and Cuenot, B.: Discrete Ordinates and Monte Carlo Methods for Radiative Transfer Simulation Applied to Computational Fluid Mechanics Combustion Modeling,, J*HT*, vol. 131, no. 5, pp. 052701-1 to 052701-9, May, 2009.

Olson, G.L., Auer, L.H., and Hall, M.L.: Diffusion, P1, and Other Approximate Forms of Radiation Transport, *JQSRT*, vol. 64, pp. 619-634, 2000.

Spuckler, C. M., and Siegel, R.: Two-Flux and Diffusion Methods for Radiative Transfer in Composite Layers, *JHT*, vol. 118, no. 1, pp. 218-222, 1996.

Tan ,Z.: Radiative Heat Transfer in Multidimensional Emitting, Absorbing, and Anisotropic Scattering Media-Mathematical Formulation and Numerical Method, JHT, vol. l1l , no. l , pp.14l -147, 1989.

Tan, Z. -M., Hsu, P. -F., Wu, S. -H., and Wu, C. -Y.: Modified YIX Method and Pseudoadaptive Angular Quadrature for Ray Effects Mitigation, *JTHT*, vol. 14, no. 3, pp. 289-296, 2000.

Tencer, J. and Howell, J.R.: A Parametric Study of the Accuracy of Several Radiative Transport Solution Methods for a Set of 2-D Benchmark Problems, *Proc. ASME 2013 Summer Heat Transfer Conf.*, Minneapolis, July 14-19, 2013 (in press, *J. Heat Transfer*.)

Wu, S. -H., Wu, C. -Y., and Hsu, P. -F.: Solutions of Radiative Heat Transfer in Nonhomogeneous Participating Media Using the Quadrature Method, HTD-vol. 332, vol. 1, pp. 101–108, 1996.

G: Numerical Integration Methods for Use with Enclosure Equations

Integration methods are now discussed for use in numerical solutions of pure radiation or combined-mode problems. For radiative exchange, the integrals are often functions of two position variables, and integration is over one or both of them. For example, the configuration factor dF_{di-dj} from position $\mathbf{r}_i$ on surface i to position $\mathbf{r}_j$ on surface j appears in the integral over surface j to obtain F_{di-j} in the form [see Equations 4.9 and 5.57 in the text]

$$F_{di-j}(\mathrm{r}_i) = \int_{Aj} dF_{di-dj}(\mathrm{r}_i, \mathrm{r}_j) = \int_{Aj} K(\mathrm{r}_i, \mathrm{r}_j) dA_j \tag{G.1}$$

Many ways can be used to numerically approximate an integral. Because the integrands in radiative enclosure formulations are usually well behaved at the end points, *closed* numerical integration forms are often used that include the end points. *Open* methods do not include the end points and can be used when end-point values are indeterminate, such as for improper integrals that yield finite values when integrated. In analyses including convection and/or conduction, the numerical integration will usually use the grid spacing imposed by the differential terms. In some situations it is sufficient to use numerical integration methods that have regular grid spacing. However, uneven spacings are often advantageous to place more points in regions where functions have large variations, or to adequately follow irregular boundaries. *Gaussian quadrature* can be used for variable grid spacing. Simpler schemes such as the *trapezoidal rule* or *Simpson's rule* may be adequate for some problems. These often employ uniform grid spacing and are closed, whereas Gaussian quadrature is open. The trapezoidal rule can readily be used with a nonuniform grid size. Textbooks on numerical methods provide detailed presentations of the many available integration methods and their relative accuracies, advantages, and disadvantages. Libraries of computer codes and computational software packages have many subroutines for single or multidimensional numerical integrations that can be applied directly.

G.1 Trapezoidal Rule

The *trapezoidal rule* is a closed numerical integration method that can easily employ a variable increment size. Consider the function in Figure G.1, where an equal grid spacing of Δz is shown for the integration range from z_0 to z_N. In the trapezoidal rule each pair of adjacent points, such as $f(x, z_j)$ and $f(x, z_{j+1})$, is connected by a straight line. Then the integral from z_j to z_{j+1} is approximated by

$$\int_{zj}^{z_{j+1}} f(x,z)dz \approx (z_{j+1} - z_j)\frac{f_j(x) + f_{j+1}(x)}{2}$$

This approximation can be made for each interval between grid points, so an irregular grid spacing can be used. For *equally sized increments,* the sum over all intervals gives the approximation

$$\int_{z_0}^{z_N} f(x,z)\,dz \approx \Delta z\left[\frac{1}{2} f_0(x) + \sum_{j=1}^{N-1} f_j(x) + \frac{1}{2} f_N(x)\right] \tag{G.2}$$

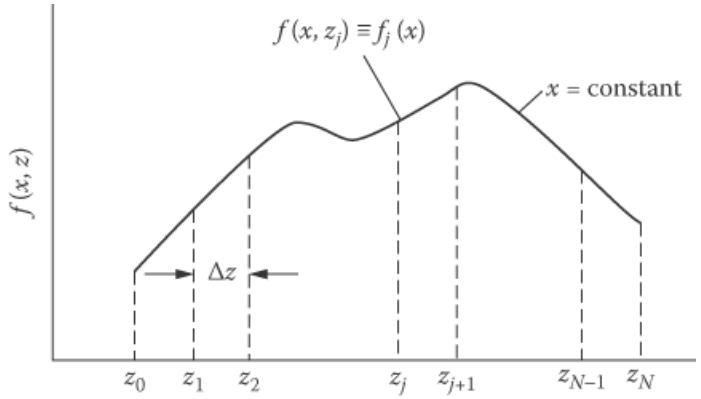

FIGURE G.1 Numerical integration of the function f(x, z) with respect to z for a fixed x.

EXAMPLE G.1

Using the ring-to-ring configuration factor, evaluate the configuration factor from a ring element on the interior of a right circular cylinder to the cylinder base for the geometry in Figure G.2 when $x = r$. Use the trapezoidal rule and compare the result with the analytical solution.

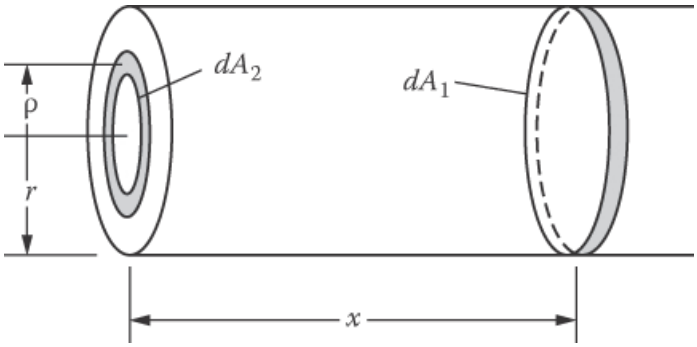

FIGURE G.2 Geometry for configuration factor from ring element on interior of cylinder to ring element on base.

The factor from dA_1 to a ring dA_2 on the base surface is

$$dF_{d1-d2}(X, R) = \frac{2XR(1 + X^2 - R^2)\,dR}{[(1 + X^2 + R^2)^2 - 4R^2]^{3/2}} \tag{G.3}$$

where $X = x/r$ and $R = \rho/r$. For this example $X = 1$, so $f_j(X = 1, R_j)$ in Figure G.1 is given by

$$f_j(X = 1, R_j) \equiv f_j(1) = \frac{2R_j(2 - R_j^2)}{(4 + R_j^4)^{3/2}}$$

where $R_j = j\Delta R$ and $\Delta R = 1/N$. In particular, letting $f_j(X=1, j\Delta R) \equiv f_j(1)$,

$$f_0(1) = 0, \quad f_j(1) = \frac{2\,j\Delta R[2-(j\Delta R)^2]}{[4+(j\Delta R)^4]^{3/2}}, \quad f_N(1) = \frac{2}{5^{3/2}}$$

These terms are substituted into Equation G.2, and for $N = 5$ yields $F_{d1-2}(X=1) = (1/5)[(1/2\times 0 + 0.09794 + 0.18225 + 0.23451 + 0.23500 + (1/2)\times 0.17889]$ $= 0.16783$

The exact configuration factor is in Appendix C of the text as

$$F_{d1-2}(X=1) = \frac{X^{*^2} + \frac{1}{2}}{(X^{*^2}+1)^{1/2}} - X^*, \quad X^* = \frac{x}{2r} = \frac{X}{2} = \frac{1}{2}$$

which gives $F_{d1-2}(X=1) = F_{d1-2}(X^*=0.5) = 0.17082$. Larger numbers of increments improve the accuracy as follows:

N	$F_{d1-2}(X=1)$	% Error
5	0.16783	−1.75
10	0.17007	−0.44
50	0.17079	−0.02
100	0.17081	−0.006
200	0.17082	0

G.2 Simpson's Rule

The usual Simpson's rule is obtained by passing a parabola through three adjacent grid points. For equally spaced increments the integral from z_j to z_{j+2} is approximated by

$$\int_{z_j}^{z_{j+2}} f(z)dz \approx \frac{\Delta z}{3}(f_j + 4f_{j+1} + f_{j+2})$$

Because this uses two Δz increments, the repeated application for a range with many grid points requires an *even* number of increments (an odd number of points). For N equally spaced increments in Figure G.1, the result is

$$\int_{z_o}^{z_N} f(z)dz \approx \frac{\Delta z}{3}(f_0 + 4f_1 + 2f_2 + 4f_3 + \cdots + 4f_{N-1} + f_N) \qquad \text{(G.4)}$$

If an odd number of increments must be used, Simpson's rule can be applied over an even number of increments, and the trapezoidal rule used for the remaining increment.

If the curve in Figure G.1 goes through a sharp cusplike peak, it may not be accurate to apply Simpson's rule if the peak is at the central point of the three adjacent points; the cusplike behavior is not accurately approximated by a parabolic curve. Simpson's rule could be used for two increments on each side of the peak. Care should be used in selecting a suitable integration scheme for each application.

Higher-order approximations have been developed by passing a cubic curve through four adjacent points, a fourth-order curve through five adjacent points, etc. These yield the *Newton-Cotes closed integration formulas* of which the trapezoidal and Simpson's rules are the first two. Using a cubic curve through four adjacent points is called *Simpson's second rule*,

$$\int_{z_j}^{z_{j+3}} f(z)dz \approx \frac{3\Delta z}{8}(f_j + 3f_{j+1} + 3f_{j+2} + f_{j+3}) \qquad \text{(G.5)}$$

G.3 Other Integration Methods

Additional numerical integration techniques include Romberg integration, in which the trapezoidal rule is utilized. The integration is performed with a small number of increments and is then repeated for twice the number of increments by adding the contributions from the additional points, four times the number of increments, etc. The sequence of integration results is extrapolated to an improved result using Richardson extrapolation [see Press et al. (1992)]. The process is continued until desired convergence accuracy is achieved in the extrapolated result.

Gaussian integration is very useful; this is an open integration method using an array of unevenly spaced points. The uneven points can be positioned between a fixed grid of evenly or variably spaced points. This can be done by curve fitting, such as by cubic splines, for the individual portions of the curve between the fixed grid points. Values of the integrand at positions between the grid points for use in the Gaussian method are interpolated using the spline coefficients.

Many numerical integration subroutines have been written for computer use and the software can be readily applied. Curve-fitting software routines are available that can be used in conjunction with Gaussian or other techniques, requiring interpolation to obtain unevenly spaced values of the function being integrated. Some subroutines perform multidimensional integrations. Computational software packages for mathematics provide numerical integration using, for example, Romberg integration, Simpson's rule, and adaptive methods; singular and infinite end points are also treated.

REFERENCE

Press, W. H., Flannery, B. P., Teukolsky, S. A., and Vetterling, W. T.: *Numerical Recipes in C: The Art of Scientific Computing*, 2d ed., Cambridge University Press, London, 1992.

H: Radiative Cooling

Under certain conditions, enhanced cooling from different types of surfaces is useful. This can be achieved via radiative cooling if the emission from the surface is enhanced at the longer wavelengths where most of the cooling (radiative energy loss) takes place. In addition, it is desirable to minimize the radiative energy gain of a given surface at the same time. This can be realized by decreasing the solar absorption and increasing the IR emission of the surface at the spectral range where it receives the radiant energy from outside. Such spectrally selective surfaces can also be useful where it is desirable to cool an object exposed to incident radiation from a high-temperature source. Common situations are objects exposed to the sun, such as a hydrocarbon storage tank, a cryogenic fuel tank in space, the roof and facades of a building, or electronic equipment which gets hot due to internal heat generation. There are several studies published over the years to enhance radiative cooling during night times {Catalanotti et al. (1975); Granqvist et al. (1982); Eriksson and Granqvist (1982); Berdahl et al.(1983); and Smith (2009) and his colleagues [Gentle et al., (2013)]}.

Few natural materials have the desired radiative responses. Radiative cooling can be enhanced using tailored properties of surfaces in both the spectral and directional sense (see Section 3.6 of the text).

The largest impact of radiative cooling would be on buildings, which consume more than one-third of the energy in the US, as well as in most energy intense countries. Air-conditioning requirements and costs are significant in buildings. If a passive system could be employed to help minimize these costs, it would be a significant help towards achieving energy efficiency. Buildings receive energy mostly from sun and emit at about room temperatures. This means that most radiation incident on buildings, which cause radiation gain, is near visible wavelengths. If the buildings themselves are assumed to be at about 300 K temperature, then their emission wavelength peaks around 10 μm, following the Wien Law. The Earth's atmosphere has a transparency window for electromagnetic waves between 8 and 13 μm that coincides with this peak thermal radiation wavelengths at these temperatures. Therefore, through this atmospheric transparency window, buildings can lose radiation quite effectively, particularly under clear sky conditions, both day and night!

A number of studies about radiative cooling are discussed by Zhu et al. (2013). It is important to achieve not only night-time cooling, but also daytime cooling. Given that there will be solar absorption during the times that cooling is most desirable, a detailed heat balance study is needed to determine a surface equilibrium temperature that is below the ambient. To achieve this, Zhu et al. have shown that it is necessary to achieve over 88 percent solar radiation reflection during the day. Yet, this approach has an architectural bottleneck, as any strong solar reflector would yield significant color change, which precludes extensive use of the idea.

To be able to do this we desire to have a 'designer' surface that has large reflectivity in the spectral region of visible (short) wavelenghts to block the peak solar energy and has large absorptivity/emissivity at far-infrared (longer) wavelengths, where the surface emission peaks. For these "spectrally/directionally selective" surfaces, we can use a performance parameter. This parameter is defined, in a very simple way, as the ratio of its directional total absorptivity $\alpha_s(\theta_i,$

ϕ_i, T_i) for incident solar energy to its hemispherical total emissivity $\epsilon(T)$ (See Equation 3.33 of the text).

In principle, a highly reflecting material, a polished metal or a metallic coated surface can be considered for these applications. Although such materials would reflect much of the incident energy at visible, they do not effectively radiate at longer wavelengths. This yields a poor desired behavior for the energy balance in the vacuum of outer space and may not provide a low α_s/ϵ. Paints, such as white paint, is an example of useful spectrally selective surfaces [Dunkle (1963)], as they do not only reflect the incident solar radiation predominant at short wavelengths, but also radiate well at the longer wavelengths characteristic of the relatively low body temperature. However, their performance should be evaluated also with convective cooling, which may dominate over radiant emission.

Cool roofs have been the prime focus of the Department of Energy in recent years. Most of this type of research is readily available on the internet.

Radiative cooling is also part of thermal control in outer space, which needs (sometimes exotic) spectrally selective surfaces. Among them, the optical solar reflector (OSR) is a mirror composed of a glass layer silvered on the back side. The glass, being transparent in the short wavelength region, $\lambda<\sim2.5\mu m$, that includes the visible range, lets the silver reflect incident radiation in this spectral region. The small fraction of short-wavelength energy that is absorbed by the silver, and the energy absorbed by the glass at longer wavelengths, are radiated away by the glass in the longer-wavelength infrared region where glass emits well.

Commonly used thin plastic sheets for solar reflection are Kapton, Mylar, and Teflon with silver or aluminum coating on the backside. Fused-silica second-surface mirrors and polished metals are essentially stable in orbit. Metalized Teflon, aluminized Kapton, and some light colored paints on the other hand, darken over a long period of time, degrading their performance as discussed by Hall and Fote (1992).

The performance of a CuO pigment coating has recently been investigated and compared against that of a white TiO_2 pigment, which is widely used as a typical white pigment (Gonome et al., 2014). They also measured results for CuO coatings and compared against the measured results for TiO_2-pigmented coating. The performance of CuO pigment was found to be much higher than that of TiO_2 pigment, though the CuO coating shows a darker, almost black color (Gonome et al., 2014). Titanium dioxide white paint is superior as an external solar-selective coating, to polyvinyl fluoride film with an aluminized coating 12 μm thick on the underside. These are the types of materials among many others that are used for spacecraft thermal control (Henninger, 1984).

The most common material system currently used for low thrust, radiation-cooled rockets or spacecrafts is a niobium alloy (C-103) with a fused silica coating (R-512A or R-512E) for oxidation protection. However, significant amounts of fuel film cooling are usually required to keep the material below its maximum operating temperature of 1370°C, degrading engine performance. Also the R-512 coating is subject to cracking and eventual spalling after repeated thermal cycling.

A new class of high-temperature, oxidation-resistant materials is being developed for radiation-cooled rocket engines, with the thermal margin to reduce or eliminate fuel film cooling,

while still exceeding the life of silicide-coated niobium. Rhenium coated with iridium is the most developed of these high-temperature materials, as discussed by Reed et al. (1993) from NASA Lewis in the early 1960s. They also studied other material systems, which may offer more thermal margin and/or oxidation resistance, such as hafnium carbide/tantalum carbide matrix composites and ceramic oxide-coated iridium/rhenium chambers. Reed et al. discussed a chamber fabricated from pure iridium that would eliminate the rhenium/iridium diffusion mechanism, but there are concerns about its structural integrity as a rocket engine. A tantalum-10% tungsten alloy and woven carbon-carbon fibers could serve as high-temperature substrates, but require a suitable oxidation-resistant coating for long life applications. Platinum-10% rhodium alloy and grain-stabilized platinum are excellent oxidation resistant materials that could be considered for very long life (tens of hours), but relatively low temperature (1650 °C) applications. Cermets and intermetallic compounds have also been considered for high temperature rocket operation, but there is a very limited experience base with them.

There are many materials that have absorption peaks at different wavelengths. Rare earth metals can be used as selective emitters in the infrared region due to their high absorption in this region [Rose et al. (1996); Licciulli et al. (2003); Wijewardane and Goswami (2012)]. Commonly, these metals are used as composites by mixing with other materials such as ceramic or titania because of the unavailability of these metals. The problem with these composites is that at higher temperatures grey-body like emission from other constituents' starts to dominate the rare earth metal's selective emission. For applications, which require peaks of various wavelengths the absorption peaks have to be tuned or shifted and the answer falls in the nano-scale. Nano sized metal particles embeded in insulators or a semiconductor matrix, as reviewed by Wijewardane and Goswami, (2012).

In addition to spectral tuning, we can also consider directional tuning of surfaces. For example, an emitting surface can be constructed to emit strongly in preferred direction, while reducing emission into unwanted directions. This approach is based on the possibility of designing a regular micro-roughness (a "grating") that would provide selective emission [Sentenac and Greffet (1994); Greffet and Henkel (2007)]. The grating dimension is of the same order of the predominant radiation wavelength. Indeed, this concept was shown experimentally and theoretically for different polarization settings [Arnold et al. (2012); see references cited). If the objective of the designer surface is to absorb primarily from a certain direction, then it can be constructed that way; also, the fabrication can be performed for it to absorb poorly in other directions. If the surface is used for solar absorption, then it would, based on the Kirchhoff law for directional properties, emit strongly toward the sun but weakly in other directions. It can absorb about the same energy as a nondirectional absorber, yet its total emission would be less than a typical surface. Coherent directional and spectral emission concepts have been explored by Greffet's group over the years [Carminati and Greffet (1999); Greffet et al. (2002); Joulain et al. (2005); Laroche et al. (2006); Arnold et al. (2012), and references therein). Recent calculations carried out by Didari and Menguc (2014) also suggest that the shape and size of the extrusions on the surfaces can alter the far-field emission. These concepts were discussed briefly in Chapter 16, and are likely to be used for selective emission in the future.

Recently, the concept of radiative cooling was explored by Fan group [Zhu et al. (2013)]. By modifying the structure of Silicon nanowire array on an Aluminum substrate, they had significant emissivity/absorptivity enhancement at far-infrared. Their feature size changed from

sub-micron to 10 nm range, and they demonstrated that the color of the sample did not change noticeably.. Zhu et al. also applied their idea of radiation cooling to solar cells, which is a very important area to enhance the performance of PV-panels [Zhu et. al. (2014)]. See also Section 8.6 of the text for further discussions and references on optimized PV cell enhancement.

REFERENCES

Arnold, C., Marquier, F., Garin, M., Pardo, F., Collin, S., Bardou, N., Pelouard, J-L., and Greffet, J.-J., Coherent Thermal Emission by Two-dimensional Silicon Carbide Gratings, *Phys. Rev. B*, vol. 86, 035316, 2012.

Berdahl, P., Martin, M., and Sakkal, F.: Thermal Performance of Radiative Cooling Panels, *IJHMT*, vol. 26, no. 6,pp. 871–880, 1983.

Carminati, R., and Greffet, J. -J.: Near-Field Effects in Spatial Coherence of Thermal Sources, *Phys. Rev. Lett.*, vol. 82, no. 8, pp. 1660–1663, 1999.

Catalanotti, S., Cuomo, V., Piro, G., Ruggi, D., Silvestrini, V., and Troise, G.: The Radiative Cooling of Selective Surfaces, *Sol. Energy*, vol. 17, 83, 1975.

Didari, A., and Mengüç, M. P.: Near-Field Thermal Emission between Corrugated Surfaces Separated by Nano-Gaps, *JQSRT*, submitted, 2014.

Dunkle, R. V.: Thermal Radiation Characteristics of Surfaces, in J. A. Clark (ed.), *Theory and Fundamental Research in Heat Transfer*, pp. 1–31, Pergamon Press, New York, 1963.

Eriksson, T. S., and Granqvist, C. G.: Radiative Cooling Computed for Model Atmospheres, *Applied Optics*, vol. 21, no. 23, 1982.

Gentle, A. R., Dybdal, K. L., and Smith, G. B.: Polymeric Mesh for Durable Infra-red Transparent Convection Shields: Applications in Cool Roofs and Sky Cooling, *Solar Energy Materials and Solar Cells*, vol. 115, pp. 79–85, 2013.

Gonome, H., Baneshi, M., Okajima, J., Komiya, A., and Maruyama, S.: Controlling the Radiative Properties of Cool Black-color Coatings Pigmented with CuO Submicron Particles, *JQSRT*, Special Issue on Micro- and Nano-scale Radiative Transfer, vol. 132, pp. 90-98, 2014.

Granqvist, C. G., Hjortsber, A., and Eriksson, T. S.: Radiative Cooling to low temperatures with selectively IR-Emitting surfaces, *Thin Solid Films*, vol. 90, pp. 187-190, 1982.

Greffet, J. -J., and Henkel, C.: Coherent Thermal Radiation, *Contemporary Phys.*, vol. 48, no. 4, pp. 183–194, July–August, 2007.

Greffet, J. -J., Carminati, R., Joulain, K., Mulet, J. -P., Mainguy, S., and Chen, Y.: Coherent Emission of Light by Thermal Sources, *Nature*, vol. 416, pp. 61–64, March 7, 2002.

Hall, D. F., and Fote, A. A.: Thermal Control Coatings Performance at Near Geosynchronous Altitude, *JTHT*, vol. 6, no. 4, pp. 665–671, 1992.

Henninger, J. H.: Solar Absorptance and Thermal Emittance of Some Common Spacecraft Thermal-Control Coatings, NASA Reference Publication 1121, 1984.

Joulain, K., Mulet, J. -P., Marquier, F., Carminati, R., and Greffet, J. -J.: Surface Electromagnetic Waves Thermally Excited: Radiative Heat Transfer, Coherence Properties and Casimir Forces Revisited in the Near Field, *Surf. Sci. Rep.*, vol. 57, pp. 59–112, 2005.

Laroche, M., Carminati, R., and Greffet, J. -J.: Near-Field Thermophotovoltaic Energy Conversion, *J. Appl. Phys.*, vol. 100, p. 063704, 2006.

Licciulli, A., Diso, D., Torsello, G., and Tundo, S.: The Challenge of High-performance Selective Emitters for Thermophotovoltaic Applications, *Semiconductor Science and Technology*, vol. 18, pp. 174-183, 2003.

Reed, B., Biaglow J., and Schneider, S.: Advanced Materials for Radiation-Cooled Rockets, in NASA Lewis Research Center, N94-23052, *NASA Propulsion Engineering Research Center, Annual Report 199, Vol. II*, NASA Lewis Research Center, N94-28052, pp. 115-118, Sept. 1993.

Rose, M. F., Adair, P., and Schroeder, K.: Selective Emitters for Thermophotovoltaic Power Systems for Use in Aerospace Applications, *J. Propul. Power*, vol. 12, no. 1, pp. 83–88, 1996.

Sentenac, A., and Greffet, J. -J.: Design of Surface Microrelief with Selective Radiative Properties, *IJHMT*, vol. 37, no. 4, pp. 553–558, 1994.

Smith, G. B.: Amplified radiative cooling via optimised combinations of aperture geometry and spectral emittance profiles of surfaces and the atmosphere, *Solar Energy Materials & Solar Cells*, vol. 93, 1696–1701, 2009.

Wijewardane, S., and Goswami, D. Y.: A Review on Surface Control of Thermal Radiation by Paints and Coatings for New Energy Applications, *Renewable and Sustainable Energy Reviews*, vol. 16, pp. 1863-1873, 2012.

Zhu, L., Raman, A., and Fan, S.: Color-preserving Daytime Radiative Cooling, *Appl. Phys. Letters*, vol. 103, 223902, 2013.

Zhu, L., Raman, A., Wang, K. X., Anoma, M. A. and Fan, S.: Radiative Cooling of Solar Cells, *Optica*, vol. 1, no. 1, July 2014.

I. RADIATION FROM FLAMES

Combustion consists of chemical reactions in series and in parallel and involving various intermediate species. The composition and concentration of these species cannot be predicted very well unless knowledge is available of the flame reaction kinetics; this detailed knowledge is not usually available or convenient to obtain. Because the flame radiation properties depend on the distributions of temperature and species within the flame, a detailed prediction of radiation from flames is not often possible from knowledge of only the combustible constituents and the flame geometry. It is usually necessary to resort to empirical methods for predicting radiative transfer in systems involving combustion.

Under certain conditions the constituents in a flame emit much more radiation in the visible region than would be expected from their gaseous absorption coefficients. For example, the typical almost transparent blue flame of a Bunsen burner can become a more highly emitting yellow-orange flame by changing the fuel-air ratio. Such luminous emission is usually ascribed to incandescent soot (hot carbon) particles formed because of incomplete combustion in hydrocarbon flames. Alternatively, Echigo et al. (1967) and others have advanced the hypothesis, supported by some experimental facts, that luminous emission from some flames is by emission from vibration-rotation bands of chemical species that appear during the combustion process *prior* to the formation of soot particles.

I.1 Radiation from Nonluminous Flames

Radiation from the nonluminous portion of the combustion products is fairly well understood. For this the complexities of the chemical reaction are not as important, since it is the gaseous end products above the active burning region that are considered. Most instances are for hydrocarbon combustion, and radiation is from the CO_2 and H_2O absorption bands in the infrared. For flames a meter or more thick, as in commercial furnaces, the emission leaving the flame within the CO_2 and H_2O vibration-rotation bands can approach blackbody emission in the band spectral regions. The gas radiation properties in Chapter 9, and the methods in this chapter, can be used to compute the radiative transfer. The analysis is greatly simplified if the medium is well mixed and can be assumed isothermal. A nonisothermal medium can be divided into approximately isothermal zones, and convection can be included if the circulation pattern in the combustion chamber is known. A nonisothermal analysis with convection was carried out in Hottel and Sarofim (1965) for cylindrical flames. In Dayan and Tien (1974), Edwards and Balakrishnan (1973), Modak (1975, 1977), Taylor and Foster (1974), and Lefebvre (1984), radiation from various types of nonluminous flames (laminar or turbulent, mixed or diffusion) is treated. The flame shape for an open diffusion flame is considered in Annamali and Durbetaki (1975). The local absorption coefficient in nonluminous flames is calculated in Grosshandler and Thurlow (1992) as a function of mixture fraction and fuel composition. Modest (2005) reviews models for radiative transfer in combustion gases.

When considering the radiation from flames, a characteristic parameter is the average temperature of a well-mixed flame as a result of the addition of chemical energy. Well-developed methods exist [Gaydon and Wolfhard (1979)] for computing the theoretical flame temperature from thermodynamic data. The effect of preheating the fuel and/or oxidizer can be included. An ideal theoretical flame temperature T is computed using energy conservation assuming complete combustion, no dissociation of combustion products, and no heat losses. The energy in the constituents supplied to the combustion process, plus the energy of combustion, is equated to the energy of the combustion products to give,

$$T - T_{ref} = \frac{\left(\text{energy in feed air and fuel above } T_{ref}\right) + \left(\text{energy released by combustion}\right)}{\left(\text{total mass of products}\right) \times \left(\text{mean specific heat of products}\right)} \quad \text{(I.1)}$$

Energy losses by radiation and other means that would lower the flame temperature are not included. Methods for including these effects are in Gaydon and Wolfhard (1979); extinction of a flame by radiative energy loss is analyzed in Ju et al. (2000). A list of ideal theoretical flame temperatures (no radiation or other losses included) is in Table I.1 for various hydrocarbon flames, using data from Gaydon and Wolfhard and from Barnett and Hibbard (1957). Results for complete combustion with dry air are shown, followed by calculated results modified to allow for product dissociation and ionization. The latter are compared with experimental results. The heats of combustion of the substances are also given. Extensive tabulations of similar data for more than 200 hydrocarbons are in Barnett and Hibbard and in Perry et al. (2007). After its average temperature has been estimated, the radiation emitted by a nonluminous flame can be considered, as illustrated by an example.

EXAMPLE I.1 As a result of combustion of ethane in 100% excess air, the combustion products are 4 mol of CO_2, 6 mol of H_2O vapor, 33.3 mol of air, and 26.3 mol of N_2. Assume these products are in a cylindrical region 4 m high and 2 m in diameter, are uniformly mixed at a theoretical flame temperature of 1853 K, and are at 1 atm pressure. Compute the radiation from the gaseous region.

The partial pressure of each constituent is equal to its mole fraction:

$$p_{CO_2} = (4/69.6)\left(1 \text{ atm}\right) = 0.0575\text{atm and } p_{H_2O} = (6/69.6)\left(1 \text{ atm}\right) = 0.0.0862\text{atm.}$$

The gas mean beam length for negligible self-absorption is, from Equation 10.107,

$$L_{e,0} = 4V/A = 4\left[\pi\left(2^2/4\right)\right] \times 4 / \left[\left(2\pi \times 4\right) + 2\pi\left(2^2/4\right)\right] = 1.6\text{m}.$$

To include self-absorption, a correction factor of 0.9 is applied to give L_e = 0.9(1.6) = 1.44 m. Then $p_{CO2}L_e$ = 0.0575 × 1.44 = 0.0828 atm · m = 8.54 bar-cm, and $p_{H2O}L_e$ = 0.0862 × 1.44 = 0.124 atm · m = 12.8 bar-cm.. Using the Leckner correlations (Equation 9.58) at 1853 K gives

ϵ_{CO2} = 0.070 and ϵ_{H2O} = 0.096 × 1.03 = 0.099. The 1.03 factor in ϵ_{H2O} is a correction for the partial pressure of the water vapor being nonzero (Equation 9.60). There is also a negative correction from spectral overlap of the CO_2 and H_2O radiation bands. This is obtained from Equation 9.63 at the values of the parameters:

$$p_{H_2O} / \left(p_{CO_2} + p_{H_2O} \right) = 0.0862 / \left(0.0575 + 0.0862 \right) = 0.60$$

$$p_{CO_2} L_e + p_{H_2O} L_e = 0.0828 + 0.124 = 0.207 \text{atm} \cdot \text{m} = 20.9 \text{bar} \cdot \text{cm}$$

The correction is $\Delta\epsilon$ = 0.031. Then the gas emittance is

$$\epsilon_g = \epsilon_{CO_2} + \epsilon_{H_2O} - \Delta\epsilon = 0.070 + 0.099 - 0.031 = 0.138 .$$

The radiation from the gas region at the theoretical flame temperature is,

$$Q = \epsilon_g \sigma T_g^4 A = 0.138 \times 5.6704 \times 10^{-8} \times 1853^4 \times 10\pi = 2900 \text{kW}$$

TABLE I.1 Heat of combustion and flame temperature for hydrocarbon fuels [Gaydon and Wolfhard (1979); Barnett and Hibbard (1957); Lide (2008)]

		Maximum flame temperature, K (combustion with dry air at 298 K)		
Fuel	Heat of combustion kJ/kg	Theoretical (complete combustion)	Theoretical (with dissociation and ionization)	Experimental
Carbon monoxide (CO)	10.1×10^4	1756	1388	
Hydrogen (H_2)	14.1×10^4	2400	2169	
Methane (CH_4)	5.53×10^4	2328	2191	2158
Ethane (C_2H_6)	5.19×10^4	2338	2244	2173
Propane (C_4H_8)	5.03×10^4	2629	2250	2203
n-Butane (C_4H_{10})	4.95×10^4	2357	2248	2178
n-Pentane (C_5H_{12})	4.53×10^4	2360	2250	
Ethylene (C_2H_4)	5.03×10^4	2523	2375	2253
Propylene (C_3H_6)	4.89×10^4	2453	2323	2213
Butylene (C_4H_8)	4.53×10^4	2431	2306	2208
Amylene (C_5H_{10})	4.50×10^4	2477		
Acetylene (C_2H_2)	5.00×10^4	2859	2607	
Benzene (C_6H_6)	4.18×10^4	2484	2363	
Toluene ($C_6H_5CH_3$)	4.24×10^4	2460	2344	

REFERENCES

Annamali, K., and Durbetaki, P.: Characteristics of an Open Diffusion Flame, *Combust. Flame*, vol. 25, pp. 137–139, 1975.

Barnett, H. C., and Hibbard, R. R. (eds.): *Basic Considerations in the Combustion of Hydrocarbon Fuels with Air*, NACA Rept. 1300, 1957.

Dayan, A., and Tien, C. L.: Radiant Heating from a Cylindrical Fire Column, *Combust. Sci. Technol.*, vol. 9, pp. 41–47, 1974.

Echigo, R., Nishiwaki, N., and Hirata, M.: A Study on the Radiation of Luminous Flames, *Eleventh Symp.* (*Int.*) *Combust.*, pp. 381–389, The Combustion Institute, 1967.

Edwards, D. K., and Balakrishnan, A.: Thermal Radiation by Combustion Gases, *IJHMT*, vol. 16, no. 1, pp. 25–40, 1973.

Gaydon, A. G., and Wolfhard, H. G.: *Flames, Their Structure, Radiation, and Temperature*, 4th ed., Chapman and Hall, London, 1979.

Grosshandler, W. L., and Thurlow, E. M.: Generalized State-Property Relations for Nonluminous Flame Absorption Coefficients, *JHT*, vol. 114, no. 1, pp. 243–249, 1992.

Lefebvre, A. H.: Flame Radiation in Gas Turbine Combustion Chambers, *IJHMT*, vol. 27, no. 9, pp. 1493–1510, 1984.

Lide, D. R. (ed.): *Handbook of Chemistry and Physics*, 88th ed., CRC Press, Boca Raton, 2008.

Modak, A.: Nonluminous Radiation from Hydrocarbon-Air Diffusion Flames, *Combust. Sci. Technol.*, vol. 10, pp. 245–259, 1975.

Modak, A.: Thermal Radiation from Pool Fires, *Combust. Flame*, vol. 29, no. 2, pp. 177–192, 1977.

Modest, M. F.: Radiative Heat Transfer Models in Combustion Gases, in *Annual Review of Heat Transfer*, Hemisphere, New York, pp. 23–47, 2005.

Perry, R. H., Green, D. W., and Maloney, J. O. (eds.): *Perry's Chemical Engineers' Handbook*, 8th ed., McGraw-Hill, New York, 2007.

Taylor, P. B., and Foster, P. J.: The Total Emissivities of Luminous and Non-luminous Flames, *IJHMT*, vol. 17, pp. 1591–1605, 1974.

Appendix J. Reviews and Historical References

Contents

J.1 General

Bone, W. A., and Townsend, D. T. A.: *Flame and Combustion in Gases*, Longmans, Green, London, 1927.

Born, M., Wolf, E., and Bhatia, A. B.: *Principles of Optics*, 7th expanded ed., Cambridge University Press, New York, 1999.

Breene, R. G.: *Theories of Spectral Line Shapes*, John Wiley and Sons, New York, 1981.

Carslaw, H. S., and Jaeger, J. C.: *Conduction of Heat in Solids*, 2d ed., Clarendon Press, Oxford, UK, 1959.

Griem, H. R.: *Principles of Plasma Spectroscopy*, Cambridge University Press, 2005.

Hecht, E.: *Optics*. 4th ed., Pearson Education, Inc., Upper Saddle River, USA, 2002.

Herzberg, G.: *Molecular Spectra and Molecular Structure*, 2d ed., 3 vols., Krieger, Malabar, FL, 1992.

Howell, J. R., Hall, M. J., and Ellzey, J. L.: Combustion of Hydrocarbon Fuels within Porous Inert Media, *Prog. Energy Comb. Science*, vol. 22, pp. 121–145, 1996.

Khalil, E. E.: *Modelling of Furnaces and Combustors*, Energy and Engineering Science Series, Gupta, A.K. and Lilley, D.G. (eds.), Abacus Press, Tunbridge Wells, U.K., 1982.

Kittel, C.: *Introduction to Solid State Physics*, John Wiley & Sons, Hoboken, 2005.

Kourganoff, V.: *Basic Methods in Transfer Problems*, Dover, New York, 1963.

Landau, L. D. and Lifshitz, E. M.: *Electrodynamics of Continuous Media*, Addison-Wesley, Reading, MA, 1960.

Maier, S. A.: *Plasmonics: Fundamentals and Applications*, Springer, New York, 2007.
Majumdar, A.: Scanning Thermal Microscopy, *Ann. Rev. of Matls Sci.*, vol. 29, pp. 505–585, 1999.
Mandel, L. and Wolf, E.: *Optical Coherence and Quantum Optics*, Cambridge University Press, Cambridge, 1995.
Mandelbrot, B. B.: *Les Objets Fractals: Forme, Hasard et Dimension*, Flammarion, Paris, 1975.
Mandelbrot, B. B.: *The Fractal Geometry of Nature*, W. H. Freeman, San Francisco, CA, 1983.
Novotny, J. L., and Hecht, B.: *Principles of Nano-optics*, University Press, Cambridge, 2006.
Patankar, S. V.: *Numerical Heat Transfer and Fluid Flow*, Hemisphere, Washington, DC, 1980.
Penner, S. S.: *Quantitative Molecular Spectroscopy and Gas Emissivities*, Addison-Wesley, Reading, MA, 1959.
Shen, J., and Tang, T.S., *Spectral and High-Order Methods with Applications*, Science Press, Beijing, 2006.
Stone, J. M.: *Radiation and Optics*, McGraw–Hill, New York, 1963.
Tien, C. L., and Cunnington, G. R.: Cryogenic Insulation Heat Transfer, in T. F. Irvine, Jr., and J. P. Hartnett (eds.), *Advances in Heat Transfer*, 9, 349–417, Academic Press, New York, 1973.
Vincenti, W. G, and Kruger Jr., C. H.: *Introduction to Physical Gas Dynamics*, Corrected Ed., Krieger Publishing Company, Malabar, FL, 1986.
Yeh, P.: *Optical Waves in Layered Media*, John Wiley & Sons, Hoboken, 2005.
Zel'dovich, Ya. B., and Raizer, Yu. P.: *Physics of Shock Waves and High-Temperature Hydrodynamic Phenomena*, vol. 1, pt. II, Academic Press, New York, 1966.

J.2 Inverse Methods

Alifanov, O. M.: *Inverse Heat Transfer Problems*, Springer, Berlin, 1994.
Alifanov, O. M., Artyukhin, E. A., and Rumyantsev, S. V.: *Extreme Methods for Solving Ill-Posed Problems with Applications to Inverse Heat Transfer Problems*, Begell House, New York, 1995.
Beck, J. V., Blackwell, B., and St. Clair, Jr., C. R.: *Inverse Heat Conduction: Ill-Posed Problems*, Wiley-Interscience, New York, 1995.
Beckman, F. S.: The Solution of Linear Equations by the Conjugate Gradient Method, in A. Ralston and H. S. Wilf (eds.), *Mathematical Methods For Digital Computers*, John Wiley and Sons, New York, 62–72, 1960.
Hansen, P. C., *Rank-Deficient and Discrete Ill-Posed Problems: Numerical Aspects of Linear Inversion*, SIAM, Philadelphia, 1998.
Kushner, H. J. and Clark, D. S.: *Stochastic Approximation Methods for Constrained and Unconstrained Systems*, Springer, New York, 1978.
Özişik, M. N., and Orlande, H. R. B.: *Inverse Heat Transfer: Fundamentals and Applications*, Taylor and Francis, New York, 2000.
Morozov, V. A.: *Methods for Solving Incorrectly Posed Problems*, Springer-Verlag, New York, 1984.
Tikhonov, A. N.: Solution of Incorrectly Formulated Problems and the Regularization Method, *Soviet Math. Dokl.*, 4, 1035–1038, 1963. [Engl. trans. *Dokl. Akad. Nauk. SSSR*, 151, 501–504, 1963.]
Vogel, C.R.: *Computational Methods for Inverse Problems*, SIAM, Philadelphia, 2002.

J.3 Radiative Transfer

J.3.1 General

Cess, R. D.: The interaction of thermal radiation with conduction and convection heat transfer, in T. F. Irvine, Jr. and J. P. Hartnett (eds.), *Advances in Heat Transfer*, vol. 1, pp. 1–50, Academic Press, New York, 1964
Frank, M. and Klar, A.: Radiative heat transfer and applications for glass production processes, in A. Farina, A. Klar, R. M. M. Mattheijj, A. Mikelić, N. Siedow, and A. Fasano (eds.), *Mathematical*

Models in the Manufacturing of Glass, Proceedings of the C.I.M.E. Summer School, pp. 57–134, Springer, Terme, Italy,2008.

Hottel, H. C.: Radiant Heat Transmission, in W. H. McAdams (ed.), *Heat Transmission*, 3d ed., McGraw-Hill, New York, 1954.

Hottel, H. C, and Sarofim, A. F.: *Radiative Transfer*, McGraw–Hill, New York, 1967.

Hottel, H. C., Sarofim, A. F., Wankat, P. C., Noble, J. J., Silcox, G. D., and Knaebel, K. S.: Heat and Mass Transfer, in D. W. Green and R. H. Perry (eds.), *Perry's Chemical Engineer's Handbook*, 8th ed., Chap. 5, pp. 5-16–5-43, McGraw-Hill, 2008.

Lee, S. -C, and Cunnington, G. R.: Theoretical Models for Radiative Transfer in Fibrous Media, in *Ann. Rev. Heat Transfer*, vol. IX, Chap. 3, pp. 159–218, Begell House, New York, 1998.

Modest, M. F.: *Radiation heat transfer*. 3rd ed., Academic Press, Waltham, MA, 2013.

Özişik, M. N.: *Radiative Transfer, and Interactions with Conduction and Convection*, John Wiley & Sons, New York, 1973.

Sparrow, E. M.: On the Calculation of Radiant Interchange between Surfaces, in W. Ibele (ed.), *Modern Developments in Heat Transfer*, pp. 181–212, Academic Press, New York, 1963b.

Sparrow, E. M., and Cess, R. D.: *Radiation Heat Transfer*, augmented edition, Hemisphere, Washington, DC, 1978.

Tencer, J. and Howell, J.R.: Coupling Radiative Heat Transfer with Other Heat Transfer Modes, *J. Brazilian Society Engng Sci*, (special edition) in prep, 2016.

Timoshenko, V. P., and Trenev, M. G.: A Method for Evaluating Heat Transfer in Multilayered Semitransparent Materials, *Heat Transfer—Sov. Res*., vol. 18, no. 5, pp. 44–57, 1986.

Viskanta, R.: Radiation Transfer and Interaction of Convection with Radiation Heat Transfer, in Thomas F. Irvine, Jr., and James P. Hartnett (eds.), *Advances in Heat Transfer*, vol. 3, pp. 175–251, Academic Press, New York, 1966.

Viskanta, R., and Anderson, E. E.: Heat Transfer in Semi-transparent Solids, in J. P Hartnett and T. F. Irvine, Jr. (eds.), *Advances in Heat Transfer*, vol. 11, pp. 317–441, Academic Press, New York, 1975.

Viskanta, R., and Mengüç, M. P.: Radiation Heat Transfer in Combustion Systems, *Prog. Energy Combust. Sci*., vol. 13, pp. 97–160, 1987.

Viskanta, R.: *Radiative Transfer in Combustion Systems: Fundamentals and Applications*, Begell House, New York, 2005.

J.3.2 Atmospheric Radiation

Bohren, C.W. and Clothiaux, E.E.: *Fundamentals of Atmospheric Radiation*, John Wiley & Sons, New York, 2006.

Coakley Jr, J. A., and Yang, P.: *Atmospheric Radiation: A Primer with Illustrative Solutions*, John Wiley & Sons, New York, 2014.

Duffie, J. A., and Beckman, W. A.: *Solar Energy Thermal Processes*, 3d ed., Wiley, New York, 2006.

Goody, R. M., and Yung, Y. L.: *Atmospheric Radiation*, 2d ed., Oxford University Press, New York, 1989.

Kondratyev, Ya. K.: *Radiation in the Atmosphere*, Academic Press, New York, 1969.

Liou, K.-N.: *An Introduction to Atmospheric Radiation*, 2nd ed., Academic Press, 2002

Petty, G.W.: *A First Course in Atmospheric Radiation*, 2nd ed., Sundog Publishing, Madison,WI., 2006.

J.3.3 Inverse solutions

Daun, K. J., Ertürk, H., and Howell, J. R.: Inverse Design Methods for High-Temperature Systems, *Arabian J. Sci. and Tech*, vol. 27, no. 2C, pp. 3–48, 2003.

Daun, K. J., Ertürk, H., Howell, J. R., Gamba, M. and Hosseini Sarvari, M.: The Use of Inverse Methods for the Design and Control of Radiant Sources, *JSME International Journal*, ser. B,

46(4), 470–478, 2003.
França, F. H. R., Howell, J. R., Ezekoye, O. A., and Morales, J. C.: Inverse Design of Thermal Systems, in J. P. Hartnett and T. F. Irvine (eds.), *Advances in Heat Transfer*, 36(1), 1–110, Elsevier, 2002.

J.3.4 k-distribution methods

André, F. and Vaillon, R.: Generalization of the *k*-moment Method Using the Maximum Entropy Principle; Application to the NBKM and Full Spectrum SLMB Gas Radiation Models, *JQSRT*, 113(12) , 1508–1520, 2012.
André, F., Solovjov, V.P., Hou, L., Vaillon, R., and Lemonnier, D.: The Generalized k-Moment Method for the Modeling of Cumulative k-Distributions of H_2O at High Ttemperature, *JQSRT* 143, 92-99, 2014a.
André, F., Hou, L., Roger, M., and Vaillon, R.: The Multispectral Gas Radiation Modeling: A New Theoretical Framework Based on a Multidimensional Approach to *k*-Distribution Methods, *JQSRT*, vol. 147, pp. 178-195, 2014b.
Howell, J. R.: Non-equilibrium Radiative Transfer Models: K-Distribution, *von Karman Institute Lecture Series STO-AVT-218-VKI, Radiation and Gas-Surface Interaction Phenomena in High-Speed Re-Entry*, University of Illinois at Urbana Champagne, April, 2014.
Modest, M.F.: The Treatment of Nongray Properties in Radiative Heat Transfer: From Past to Present, *JHT*, 135(6) 061801-1 through 061801-12. doi:10.1115/1.40235, 2013.

J.3.5 Mathematical Resources

Abramowitz, M. and Stegun, I. A.: *Handbook of Mathematical Functions*, Dover, New York, 1965.
Altaç, Z.: Integrals Involving Bickley and Bessel Functions in Radiative Transfer, and Generalized Exponential Integral Functions, *JHT*, vol. 118, no. 3, pp. 789–792, 1996.
Breig, W. F., and Crosbie, A. L.: Numerical Computation of a Generalized Exponential Integral Function, *Math. Comput*., vol. 28, no. 126, pp. 575–579, 1974.
Chang, S. L., and Rhee, K. T.: Blackbody Radiation Functions, *Int. Comm. Heat Mass Transfer*, vol. 11, pp. 451–455, 1984.
Chung, T. J.: Integral and integrodifferential systems, in W. J. Minkowitz, E. M. Sparrow, G. E. Schneider, and R. H. Pletcher (eds.), *Handbook of Numerical Heat Transfer*, Chapter 14, Wiley, New York, 1988.

J.3.6 Microscale-Nanoscale

Basu, S., Chen, Y.B., and Zhang, Z.M.: Microscale Radiation in Thermophotovoltaic Devices- A Review, *Int. J. Energy Research*, vol. 31, no. 6-7, pp. 689-716 , 2007.
Boltasseva, A., and Shalaev, V.: Fabrication of Optical Negative-index Metamaterials: Recent Advances and Outlook, *Metamaterials*, vol. 2, pp. 1-17, 2008.
Cai, W. and Shalaev, V.: *Optical Metamaterials: Fundamentals and Applications*, Springer, New York, 2010.
Carey, V. P., Chen, G., Grigoropoulos, C., Kaviany, M., and Majumdar, A.: A Review of Heat Transfer Physics, *Nanosc. Microsc. Therm.*, vol. 12, pp. 1–60, 2008.
Chen, G.: *Nanoscale Energy Transport and Conversion*, Oxford University Press, New York, 2005.
Cahill, D.G., Ford, W.K., Goodson, K.E., Mahan, G.D., Majumdar, A., Maris, H.J., Merlin, R., and Phillpot, S.R.: Nanoscale thermal transport, *J. Appl. Phys*. vol. 93, pp. 793–818, 2003.
Cahill, D.G. et al.: Nanoscale thermal transport II. 2003–2012, *Appl. Phys. Revs*, vol. 1, 011305, 2014.
Corbitt, S., Francoeur, M., and Raeymaekers, B.:Implementation of Optical Dielectric Metamaterials: A Review," *JQSRT*, **158**, 3-16, 2015.

Francoeur, M.: Thermal fundamentals, Chap. 4 in *Micro Energy Harvesting*, Briand,D., Yeatman, E. and Roundy,S. (eds.) Wiley-VCH, 2015.

Greffet, J. -J., Carminati, R., Joulain, K., Mulet, J. -P., Mainguy, S., and Chen, Y.: Coherent Emission of Light by Thermal Sources, *Nature*, vol. 416, pp. 61–64, March 7, 2002.

Hajimirza, S., Heltzel, A., and Howell, J.R.: Optimizing Nanoscale Surface Properties for Enhancing Radiative Energy Control, *Prog. Energy Combustion Sci*., in prep., 2016.

Liu, X., Wang, L., and Zhang, Z.M.: Near-Field Thermal Radiation: Recent Progress and Outlook, *Nanoscale and Microscale Thermophysical Engineering*, 19(2), 98-126, 2015

Narayanaswamy, A., and Chen, G.: Direct Computation of Thermal Emission from Nanostructures, *Ann. Rev. Heat Transfer*, vol. 14, pp. 169–195, 2005b.

Raether, H.: *Surface Plasmons on Smooth and Rough Surfaces and on Gratings*, Springer-Verlag, Berlin, 1988.

Rytov, S. M.: *Theory of Electric Fluctuations and Thermal Radiation*, Air Force Cambridge Research Center, Bedford, MA, 1959.

Rytov, S. M., Kravtsov, Y. A., and Tatarskii, V. I.: *Principles of Statistical Radiophysics 3: Elements of Random Fields*, Springer, Berlin, Heidelberg, New York, 1989.

Shi, L., Dames, C., Lukes, J.R., Reddy, P., Duda, J., Cahill, D.G., Lee, J., Marconnet, A., Goodson, K.E., Bahk, J.-H., Shakouri, A., Prasher, R.S., Felts, J., King, W.P., Han, B., and Bischof, J.C.: Evaluating Broader Impacts of Nanoscale Thermal Transport Research, *Nanoscale and Microscale Thermophysical Engineering*, 19(2), 127-165, 2015

Taflove, A.: *Advances in FDTD Techniques and Applications in Photonics*, *Photonics North 2007*, Ottawa, Ontario, Canada, June 4, 2007.

Wong, B. T. and Mengüç, M. P.: *Thermal Transport for Applications in Micro- and Nanomachining*, Springer, Berlin, Germany, 2008.

Zhang, Z. M.: *Nano/Microscale Heat Transfer*, McGraw-Hill, New York, 2007.

J.3.7 Properties

Fox, M: *Optical Properties of Solids*, Oxford University Press, Oxford, UK, 2001.

Palik, E. D. (ed.): *Handbook of Optical Constants of Solids*, vols. I-IV, Elsevier, New York, 1998.

Reed, B., Biaglow, J., and Schneider, S.: *Advanced Materials for Radiation-Cooled Rockets*, vol. II, pp. 115–118, NASA Propulsion Engineering Research Center, Annual Report 199, NASA Lewis Research Center, N94-28052, Washington, DC, September 1993.

Rothman, L. S., Jacquemart, D., Barbe, A., et al.: The *HITRAN* 2004 Molecular Spectroscopic Database, *JQSRT*, vol. 96, pp. 139–204, 2005. For most recent version (2012) see http://www.cfa.harvard.edu/hitran//.

Rothman, L.S., Gordon, I.E., Barber, R.J., Dothe, H., Gamache, R.R., Goldman, A., Perevalov, V., Tashkun, S.A., and Tennyson, J.: "HITEMP, the High-temperature Molecular Spectroscopic Database," *JQSRT*, vol. 111, no. 15, 2139.2150 , 2010.

Svet, D. I.: *Thermal Radiation; Metals, Semiconductors, Ceramics, Partly Transparent Bodies, and Films*, Consultants Bureau, Plenum Publishing, New York, 1965.

Tien, C. L.: Thermal Radiation Properties of Gases, in T. F. Irvine, Jr., and J. P. Hartnett (eds.), *Advances in Heat Transfer*, vol. 5, pp. 253–324, Academic Press, New York, 1968.

Touloukian, Y. S., and Ho, C. Y. (eds.): Thermophysical Properties of Matter, TRPC Data Services. Volume 7, *Thermal Radiative Properties: Metallic Elements and Alloys*, Touloukian, Y. S. and DeWitt, D. P. (1970); Volume 8, *Thermal Radiative Properties: Nonmetallic Solids*, Touloukian, Y. S. and DeWitt, D. P. (1972a); Volume 9, *Thermal Radiative Properties: Coatings*, Touloukian, Y. S., DeWitt, D. P., and Hernicz, R. S. (1972b), Plenum Press, New York.

Wood, W. D., Deem, H. W., and Lucks, C. F.: *Thermal Radiative Properties*, Plenum Press, New York, 1964.

J.3.8 RTE Solution Methods

J.3.8.1 Finite Element

Nice, M. L.: Application of Finite Element Method to Heat Transfer in a Participating Medium, in T. M. Shih (ed.), *Numerical Properties and Methodologies in Heat Transfer*, pp. 497–514, Hemisphere, Washington, DC, 1983.

J.3.8.2 Finite Volume

Chai, J. C., and Patankar, S. V.: Finite Volume Method for Radiation Heat Transfer, in W. Minkowycz, and E. Sparrow (eds.), *Advances in Numerical Heat Transfer*, vol. 2, Taylor and Francis, London, 2000.

Mathur, S. R., and Murthy, J. Y.: Unstructured Finite Volume Methods for Multi-mode Heat Transfer, in W. J. Mincowycz and E. M. Sparrow (eds.), *Advances in Numerical Heat Transfer*, vol. 2, pp. 37–70, Taylor and Francis, New York, 2000.

J.3.8.3 Monte Carlo

Burns, P. J. and Pryor, D. V.: Surface radiative transport at large scale via Monte Carlo, in C.-L. Tien (ed.), *Annual Review of Heat Transfer*, IX, Chapter 7, pp. 79–158, Begell House, New York, 1998.

Cashwell, E. D. and Everett, C. J.: *A Practical Manual on the Monte Carlo Method for Random Walk Problems*,Pergamon, New York, 1959.

Farmer, J. T., and Howell, J. R.: Monte Carlo Strategies for Radiative Transfer in Participating Media, in J. P. Hartnett and T. Irvine, (eds.), *Advances in Heat Transfer*, vol. 31, pp. 1–97, Acadamic Press, San Diego, 1998.

Haji-Sheikh, A., and Sparrow, E. M.: Probability Distributions and Error Estimates for Monte Carlo Solutions of Radiation Problems, in T. F. Irvine, W. E. Ibele, J. P. Hartnett, and R. J. Goldstein (eds.), *Progress in Heat and Mass Transfer*, vol. 2, pp. 1–12, Pergamon, Oxford, 1969.

Haji-Sheikh, A.: Monte Carlo Methods, in W. J. Minkowycz, E. M. Sparrow, G. E. Schneider, and R. H. Pletcher (eds.), *Handbook of Numerical Heat Transfer*, Chap. 16, pp. 672–723, Wiley Interscience, New York, 1988

Haji-Sheikh, A., and Howell, J. R.: Monte Carlo Methods, in W. J. Minkowycz, E. M. Sparrow, and J. Y. Murthy (eds.), *Handbook of Numerical Heat Transfer*, 2d ed., Chap. 8, pp. 249–296, Wiley Interscience, New York, 2006.

Halton, J. H.: A Retrospective and Prospective Survey of the Monte Carlo Method, *SIAM Rev*., vol. 12, no. 1, pp. 1–63, 1970.

Hammersley, J. M., and Handscomb, D. C.: *Monte Carlo Methods*, Wiley, New York, 1964.

Metropolis, N., and Ulam, S.: The Monte Carlo Method, *J. Am. Stat. Assoc*., vol. 44, no. 247, pp. 335–341, 1949.

Schreider, Yu. A. (ed.): *Method of Statistical Testing—Monte Carlo Method*, American Elsevier, New York, 1964.

Taussky, O. and Todd, J.: Generating and testing of pseudo-random numbers, in H. A. Meyer (ed.), *Symposium on Monte Carlo Methods*, pp. 15–28, Wiley, New York, 1956.

Walters, D. V., and Buckius, R. O.: Monte Carlo Methods for Radiative Heat Transfer in Scattering Media, in C. -L. Tien (ed.), *Annual Review of Heat Transfer*, vol. 5, Chap. 3, pp. 131–176, CRC Press, Boca Raton, 1994.

Wing, G. W.: *A Primer on Integral Equations of the First Kind*, SIAM, Philadelphia, 1991.

Yang, W. -J., Taniguchi, H., and Kudo, K.: Radiative Heat Transfer by the Monte Carlo Method, in J. P. Hartnett and T. F. Irvine (eds.), *Advances in Heat Transfer*, vol. 27, pp. 1–215, Academic Press, San Diego, 1995.

Yarbrough, D. W., and Lee, C. -L.: Monte Carlo Calculation of Radiation View Factors, in F. R. Payne et al. (eds.), *Integral Methods in Science and Engineering 85*, pp. 563–574, Hemisphere, Washington, DC, 1985.

J.3.9 Scattering

Baillis, D., and Sacadura, J.F., Thermal Radiation Properties of Dispersed Media: Theoretical Prediction and Experimental Characterization, *JQSRT* 67, 327-363, 2000.

Barber, P. W., and Hill, S. S.: *Light Scattering by Particles: Computational Methods*, World Scientific, Singapore, 1990.

Bayvel, L. P., and Jones, A. R.: *Electromagnetic Scattering and Its Applications*, Applied Science, London, pp. 5–6, 1981.

Beckmann, P., and Spizzichino, A.: *The Scattering of Electromagnetic Waves from Rough Surfaces*, Macmillan, New York, 1963.

Bohren, C., and Huffman, D.: *Absorption and Scattering of Light by Small Particles*, Wiley-Interscience, New York, 1983.

Charalampopoulos, T. T.: Morphology and dynamics of agglomerated particulates in combustion systems using light scattering techniques, *Prog. Energy Combust. Sci.*, 18, 13–45, 1992.

Doicu, A., Wriedt, T., and Eremin, Y. A.: *Light Scattering by Systems of Particles*, Springer, Heidelberg, 2006.

Dombrovsky, L. A. and Baillis, D.: *Thermal Radiation in Disperse Systems: An Engineering Approach*, Begell House, Redding, PA, 2010.

Henyey, L. G., and Greenstein, J. L.: Diffuse Radiation in the Galaxy, *Astrophys. J.*, vol. 88, pp. 70–83, 1940.

Kerker, M.: *The Scattering of Light and Other Electromagnetic Radiation*, Academic Press, New York, 1961.

Mie, G.: Beiträge zur Optik trüber Medien, speziell kolloidaler Metallösungen, *Ann. Phys.*, vol. 330, pp. 377–445, 1908.

Mie, G.: Optics of Turbid Media, *Ann. Phys.*, vol. 25, no. 3, pp. 377–445, 1908.

Mishchenko, M. I., Hovenier, J. W., and Travis, L. D.: *Light Scattering by Nonspherical Particles*, Academic Press, New York, 2000.

Mishchenko, M. I., Travis, L. D., and Lacis, A. A.: *Scattering, Absorption, and Emission of Light by Small Particles*, Cambridge University Press, London, 2002.

Mishchenko, M. I., Travis, L. D., and Lacis, A. A.: *Multiple Scattering of Light by Particles: Radiative Transfer and Coherent Back Scattering*, Cambridge Press, New York, 2006.

Rayleigh, Lord: On scattering of light by small particles, *Philos. Mag.*, 41, 447–454, 1871.

Rayleigh, Lord: On the incidence of electric and aerial waves upon small obstacles in the form of ellipsoids or elliptic cylinders and on the passage of electric waves through a circular aperture in a conducting screen, *Phil. Mag.*, 44, 28–52, 1897.

Rother, T.: *Electromagnetic Wave Scattering on Nonspherical Particles, Basic Methodology and Simulations*, Springer Series Optical Sciences, 2009.

Schuerman, D. W. (ed.): *Light Scattering by Irregularly Shaped Particles*, Plenum Press, State University of New York at Albany, NY, 1979.

Stokes, G. G.: On the Composition and Resolution of Streams of Polarized Light from Different Sources, *Trans. Camb. Phil. Soc.*, vol. 9, pp. 399–424, 1852. (Reprinted in *Mathematical and Physical Papers*, vol. 3, Cambridge University Press, pp. 233–258, London, 1901.)

Tang, K., Yang, Y., and Buckius, R. O.: Theory and Experiments on Scattering from Rough Interfaces, in C. -L. Tien (ed.), *Annual Review of Heat Transfer*, vol. X, Chap. 3, pp. 101–140, Begell House, 1999b.

Tien, C. L., and Drolen, B. L.: Thermal Radiation in Particulate Media with Dependent and Independent Scattering, *Annual Review of Numerical Fluid Mechanics and Heat Transfer*, vol. 1, pp. 1–32, Hemisphere, Washington, DC, 1987.

Tsang, L., Kong, J. A., and Ding, K. H.: *Scattering of Electromagnetic Waves*, Wiley, New York, 2000.

Van de Hülst, H. C: *Light Scattering by Small Particles*, Wiley, New York, 1957; Dover Publications, New York, 1981.

Xu, R.: *Particle Characterization: Light Scattering Methods*, Springer, 2001.

J.4 Historical References

Agassi, J.: The Kirchhoff-Planck Radiation Law, *Science*, 156, pp. 30-37, April, 1967.

Ambarzumian, V. A.: Diffusion of Light by Planetary Atmospheres, *Astron. Zh*., vol. 19, pp. 30–41, 1942.

Aschkinass, E.: Heat Radiation of Metals, *Ann. Phys*., 17, no. 5, pp. 960–976, 1905.

Barr, E. S.: Historical Survey of the Early Development of the Infrared Spectral Region, *Am. J. Phys*., 28, no. 1, pp. 42–54, 1960.

Boltzmann, L.: Ableitung des Stefan'schen Gesetzes, betreffend die Abhängigkeit der Wärmestrahlung von der Temperatur aus der electromagnetischen Lichttheorie, *Ann. Phys*., ser. 2, vol. 22, pp. 291–294, 1884.

Chandrasekhar, S.: *Radiative Transfer*, Dover, New York, 1960.

Charle, M.: *Les Manuscripts de Léonard de Vinci, Manuscripts C, E, et K de la Bibliothèque de l'Institute Publiés en Facsimilés Phototypiques*, Ravisson-Mollien, Paris. 1888. (Referenced in Knowles Middleton, W. E.: Note on the Invention of Photometry, *Am. J. Phys*., vol. 31, no. 3, pp. 177–181, 1963.)

Crepeau, J.: A Brief History of the T^4 Law, *Proc. HT 2009; 2009 Summer Heat Transfer Conf*., Paper HT2009-88060, San Francisco, July, 2009.

d'Aguillon, F., S. J.: Opticorum Libri Sex, Antwerp, 1613. (Referenced in Knowles Middleton, W. E.: Note on the Invention of Photometry, *Am. J. Phys*., 31, no. 3, pp. 177–181, 1963.)

Davisson, C, and Weeks, J. R., Jr.: The Relation between the Total Thermal Emissive Power of a Metal and Its Electrical Resistivity, *JOSA*, 8, no. 5, pp. 581–605, 1924.

Draper, J. W.: On the Production of Light by Heat, *Phil. Mag*., ser. 3, vol. 30, pp. 345–360, 1847.

Eckert, E.: Das Strahlungsverhaltnis von Flachen mit Einbuchtungen und von zylindrischen Bohrungen, *Arch. Waermewirtsch*., vol. 16, no. 5, pp. 135–138, 1935.

Eddington, A. S.: *The Internal Constitution of the Stars*, Cambridge University Press, 1926.

Gardon, R.: A Review of Radiant Heat Transfer in Glass, *J. Am. Ceram. Soc.*, 44(7), pp. 305–312, 1961.

Hagen, E. and Rubens, H.: Metallic reflection, *Ann. Phys.*, 1(2), 352–375, 1900. (See also E. Hagen and H. Rubens: Emissivity and electrical conductivity of alloys, *Deutsch. Phys. Ges. Verhandl*., 6(4), 128–136, 1904.)

Herschel, William; Investigation of the Powers of the prismatic Colours to heat and illuminate Objects; with Remarks, that prove the different Refrangibility of Radiant Heat. To which is added, an Inquiry into the Method of viewing the Sun advantageously, with Telescopes of large Apertures and high magnifying Powers, *Trans. Roy. Soc. (London)*, 90, Pt. II, pp. 255-326 plus 16 plates, 1800.

Horvath, H.: Gustav Mie and the Scattering and Absorption of Light by Particles: Historic Development and Basics, *JQSRT*, 110, no. 11, pp. 787–799, July, 2009.

Horvath, H., (ed.): Light Scattering: Mie and More–Commemorating 100 Years of Mie's 1908 Publication, *JQSRT Special Issue*, 110, no. 11, 2009b.

Jeans, Sir J.: On the Partition of Energy between Matter and the Ether, *Phil. Mag*., vol. 10, pp. 91–97, 1905.

Langley, S. P.: Experimental Determination of Wave-Lengths in the Invisible Prismatic Spectrum, *Mem. Natl. Acad. Sci*., 2, pp. 147–162, 1883.

Lewis, H. R.: Einstein's Derivation of Planck's Radiation Law, *Am. J. Phys*., 41(1), pp. 38–14, 1973.

Lilienfeld, P.: Gustav Mie: The Person, *Appl. Opt*., 30, no. 33, pp. 4696–4698, 1991.

Lorenz, L.: Lysbevaegelsen i og uden for en af plane Lysbolger belyst Kugle, *Det Kongelige Danske Videnskabernes Selskabs Skrifter*, 6. Raekke, 6. Bind, 1890, 1, pp. 1–62. (see Classical Papers at http://www.t-matrix.de/)

Lorenz, L: Sur la lumière réfléchie et réfractée par une sphère (surface) transparente, in Oeuvres scientifiques de L. Lorenz." revues et annotées par H. Valentiner. Tome Premier, Libraire Lehmann & Stage, Copenhague, 1898, pp. 403–529. (see Classical Papers at http://www.t-matrix.de/)

J: Reviews and Historical References

Lummer, O. and Pringsheim, E., *Verhandl. Der Deutschen Physikal. Gesells*., 1, 23 and 215, 1899.

Lummer, O. and Pringsheim, E., *Verhandl. Der Deutschen Physikal. Gesells.*, 2, 163, 1900.

Maxwell, J. C.: A Dynamical Theory of the Electromagnetic Field, in W. D. Niven (ed.), *The Scientific Papers of James Clerk Maxwell*, vol. 1, Cambridge University Press, London, 1890.

Metropolis, N., and Ulam, S.: The Monte Carlo Method, *J. Am. Stat. Assoc*., 44, no. 247, pp. 335–341, 1949.

Mie, G.: Beiträge zur Optik trüber Medien, speziell kolloidaler Metallösungen, *Ann. Phys.*, vol. 330, pp. 377–445, 1908.

Mie, G.: Optics of Turbid Media, *Ann. Phys*., 25, no. 3, pp. 377–445, 1908.

Milne, F. A.: Thermodynamics of the Stars, in *Handbuch der Astrophysik*, 3, pp. 65–255, Springer-Verlag, OHG, Berlin, 1930.

Mott, N. F., and Zener, C.: The Optical Properties of Metals, *Cambridge Philos. Soc. Proc*., pt. 2, vol. 30, pp. 249–270, 1934.

Nobili, L. and Melloni, M.: New Experiments in Caloric, performed by means of the Thermomultiplier," *Am. J. Sci. and Arts*, , no. 1, pp. 185-180, 1833. (Trans. from *Annales de Chim. et de Phys.*, Oct., 1831.)

Nusselt, W.: Graphische Bestimmung des Winkelverhaltnisses bei der Wärmestrahlung, *VDI Z.*, vol. 72, p. 673, 1928.

Park, D. and Epstein, H.T.: On the Planck Radiation Formula, *Am. J. Phys*., vol. 17, pp. 301-302, 1949.

Planck, M.: Distribution of Energy in the Spectrum, *Ann. Phys*., vol. 4, no. 3, pp. 553–563, 1901.

Planck, Max: *The Theory of Heat Radiation*, 2nd. ed. (trans. by M. Masius), Dover, New York, 1959.

Poljak, G.: Analysis of the Heat Exchange by Radiation Between Gray Surfaces by the Saldo Method, *Tech. Phys. USSR*, 1, no. 5/6, pp. 555-590, 1935.

Rayleigh, Lord: On Scattering of Light by Small Particles, *Philos. Mag.*, 41, pp. 447–454, 1871.

Rayleigh, Lord: The Law of Complete Radiation, *Phil. Mag*., 49, pp. 539–540, 1900.

Rosseland, S.: *Theoretical Astrophysics: Atomic Theory and the Analysis of Stellar Atmospheres and Envelopes*, Clarendon Press, Oxford, 1936.

Schuster, A.: Radiation through a Foggy Atmosphere, *Astrophys. J*., 21, pp. 1–22, 1905.

Schwarzschild, K.: Equilibrium of the Sun's Atmosphere, *Ges. Wiss. Gottingen Nachr., Math-Phys. Klasse*, vol. 1, pp. 41–53, 1906.

Saunders, O. A.: Notes on Some Radiation Heat Transfer Formulae, *Proc. Phys. Soc. London*, 41, pp. 569–575, 1929.

Schmidt, E., and Eckert, E. R. G.: Über die Richtungsverteilung der Wärmestrahlung von Oberflächen, *Forsch. Geb. Ingenieurwes*., 6(4), pp. 175–183, 1935.

Stefan, J.: Über die beziehung zwischen der wärmestrahlung und der temperatur, *Sitzber. Akad. Wiss. Wien*, 79(2), 391–428, 1879.

Stokes, G. G.: On the Composition and Resolution of Streams of Polarized Light from Different Sources, *Trans. Camb. Phil. Soc*., vol. 9, pp. 399–424, 1852. (Reprinted in *Mathematical and Physical Papers*, vol. 3, Cambridge University Press, pp. 233–258, London, 1901.)

Townsend, A. A.: The Effects of Radiative Transfer on Turbulent Flow of a Stratified Fluid, *J. Fluid Mech.* vol. 4, no. 4, pp. 361-375, Aug., 1958.

Wien, W.: Temperatur und Entropie der Strahlung, *Ann. Phys*., ser. 2, vol. 52, pp. 132–165, 1894.

Wien, W.: Über die Energievertheilung im Emissionsspectrum eines schwarzen Körpers, *Ann. Phys*., ser. 3, vol. 58, pp. 662–669, 1896.

Zerefos, C. S., Tetsis, P., Kazantzidis, A., Amiridis, V., Zerefos, S.C.. Luterbacher, J., Eleftheratos, K., Gerasopoulos, E., Kazadzis, S., and Papayannis, A.: Further evidence of important environmental information content in red-to-green ratios as depicted in paintings by great masters, *Atmos. Chem. Phys*.14, 2987-3015, 2014.